

# The Shape and Scale of Galactic Rotation from Cepheid Kinematics

Mark R. Metzger<sup>1,2</sup>

Physics Department, Room 6-216, Massachusetts Institute of Technology,  
Cambridge, MA 02139

John A. R. Caldwell

South African Astronomical Observatory, Observatory 7935, South Africa

and

Paul L. Schechter

Physics Department, Room 6-206, Massachusetts Institute of Technology,  
Cambridge, MA 02139

## ABSTRACT

A catalog of Cepheid variables is used to probe the kinematics of the Galactic disk. Radial velocities are measured for eight distant Cepheids toward  $\ell = 300^\circ$ ; these new Cepheids provide a particularly good constraint on the distance to the Galactic center,  $R_0$ . We model the disk with both an axisymmetric rotation curve and one with a weak elliptical component, and find evidence for an ellipticity of  $0.043 \pm 0.016$  near the Sun. Using these models, we derive  $R_0 = 7.66 \pm 0.32$  kpc and  $v_{circ} = 237 \pm 12$  km s<sup>-1</sup>. The distance to the Galactic center agrees well with recent determinations from the distribution of RR Lyrae variables, and disfavors most models with large ellipticities at the solar orbit.

*Subject headings:* Cepheids — Galaxy: fundamental parameters — Galaxy: kinematics and dynamics — Galaxy: structure — distance scale — techniques: radial velocities

## 1. Introduction

The first use of Cepheids to measure kinematic parameters of the rotation curve was by Joy (1939), who found a distance to the Galactic center of 10 kpc; this distance was inferred from the measured shape of the rotation curve assuming a simple model. Cepheids have several significant

---

<sup>1</sup>Present Address: California Institute of Technology, Mail Code 105-24, Pasadena, CA 9115

<sup>2</sup>Email: [mrm@grus.caltech.edu](mailto:mrm@grus.caltech.edu)

advantages over other stellar tracers for determining large-scale Galactic kinematics. They are intrinsically bright ( $M_V \simeq -4.1$ ), which in conjunction with variability makes them relatively easy to locate at large distances. Perhaps the most significant advantage of Cepheids is that distances to them can be determined extremely well: modern calibrations of the period-luminosity relation in the near infrared yield uncertainties of  $< 5\%$  (Madore & Freedman 1991). Distances to Cepheids in the Galactic disk can be best obtained from near-infrared photometry, due both to the smaller PL relation scatter and because of heavy extinction by dust in the Galactic plane.

Further studies were carried out by Stibbs (1956), Kraft & Schmidt (1963), and Feast (1967), using additional data on Cepheids and incorporating the use of individual reddenings in distance measurements. Their analysis was ultimately limited, however, by the small amount of available data, particularly on distant, faint Cepheids. Caldwell & Coulson (1987, hereafter CC) made an extensive compilation of available Cepheid photometry and radial velocities, and used the data in an axisymmetric rotation curve model to determine, among other parameters, the distance to the Galactic center ( $R_0$ ). Though a significant improvement over earlier work, their models were also limited by the available data: CC lamented that many distant Cepheids lacked good radial velocities, and there were few Cepheids known at large distances from the sun, particularly toward directions which provide the best constraints on  $R_0$ .

More recently, new radial velocities for many distant Cepheids have been measured (Metzger *et al.* 1991, Metzger, Caldwell, & Schechter 1992, Pont *et al.* 1994b), and used in models by Caldwell *et al.* (1992) and Pont, Mayor, & Burki (1994a, hereafter PMB). Uncertainties in the parameters of the axisymmetric rotation curve models employed, including  $R_0$ , were significantly improved. Under the assumptions made by the models, it is one of the most precise ways to measure  $R_0$  (Reid 1993).

Many studies suggest, however, that the simple axisymmetric picture of Galactic rotation may not be correct. Much evidence leads to the conclusion that the Milky Way is a barred spiral (e.g. Blitz & Spergel 1991b, Binney *et al.* 1991, Weinberg 1992, Dwek *et al.* 1995), and there are suggestions that even orbits near the Sun are significantly elliptical (e.g. Blitz & Spergel 1991a, Kuijken & Tremaine 1994). A curious result of many rotation models using Cepheids, first noted by Joy (1939), has been an apparent constant velocity offset of  $\approx 3 \text{ km s}^{-1}$  between mean Cepheid velocities and the local standard of rest (LSR). Though the Cepheid sample has grown and measurements have improved for recent studies, this term has persisted. Some explanations for this effect have included a possible error in radial velocity zero-point or an artifact of measuring velocities in a pulsating atmosphere (CC). One of the results of the PMB study was to suggest that instead this velocity offset might be a kinematic effect explained by a bar-driven ellipticity of the solar orbit.

In this paper, we present new data on eight distant Milky Way Cepheids discovered by Caldwell, Keane, & Schechter (1991). These Cepheids are located near the solar circle, which gives them high leverage in determining  $R_0$  and helps to decouple the measurement of  $R_0$  from the local

rotation speed. We combine the new data with a catalog of Galactic Cepheid data, and measure new Galactic rotation parameters using an axisymmetric model. We also study the kinematics using the non-axisymmetric models of Kuijken & Tremaine (1994), and measure a component of the local potential ellipticity.

## 2. Velocities for New Cepheids

Caldwell, Keane, & Schechter (1991) conducted a search for distant Milky Way Cepheids in an area near  $\ell = 300^\circ$ ,  $b = 0^\circ$  covering 9.4 square degrees. From over 2000 variable stars identified in the survey, 37 were chosen as promising Cepheid candidates. The candidates were selected based on sparse I-band data, which could not provide a firm classification of the candidates. Additional multi-band photometry of the candidates was obtained to help confirm the identity of these stars (Avruch 1991).

We obtained spectra for many of the candidates in February 1991 at Las Campanas, both to help establish these candidates as Cepheids and to obtain radial velocities for use in kinematic models. To select the most promising candidates for frequent observation, we made use of V- and I-band followup photometry of Avruch (1991). I-band data from the original survey were combined with new observations to generate a detailed light curve, and new V-band observations were used to provide color information at different pulsational phases. Since Cepheids have a characteristic  $(V - I)$  color change over the course of pulsation (e.g. Moffett & Barnes 1985), we ranked the candidates for observation based on the slope of  $dV/dI$  as well as the appearance of the I-band light curve.

### 2.1. Observations and Data Reduction

Spectra of the candidates were taken with the Modular Spectrograph on the DuPont 2.5m telescope at Las Campanas on the nights of 25 February through 2 March 1991. We used the spectrograph in a cross-dispersed mode with a 150  $\ell/\text{mm}$  immersion grating and a 300  $\ell/\text{mm}$  grism cross-disperser, projected onto a TI 800 $\times$ 800 CCD. The primary disperser was adjusted to place orders 14–25 onto the CCD, providing coverage from 5000–8700 Å. A 1.0 arcsec slit was used throughout the run, which projected to 2.2 pixels on the detector at 8400 Å and gave an effective resolution of 60 km s<sup>-1</sup>. Calibration frames were taken after each stellar spectrum using He-Ne and Fe-Ar lamps.

The data reduction was conducted using a slightly modified version of the procedure described by Metzger *et al.* (1991). Each spectrum was flattened using an incandescent lamp exposure, and strong cosmic ray events were removed. Calibration lines from the associated lamp exposures were identified and centroided using a modified version of DoPHOT (Mateo & Schechter 1989), and fit across orders with a fifth-order 2-dimensional Legendre polynomial. The high-order coefficients

were fixed using a long lamp exposure that yielded over 300 identified lines, and the 4 lowest-order coefficients were fit to each calibration frame, which typically had 100 available lines. Each stellar spectrum was rebinned in  $\log\lambda$  according to the calibration, and each order was separately extracted and sky-subtracted.

During the course of the reduction, we noticed that the spectrum shifted abruptly between two positions on the chip throughout the observing run. The shift was aligned in the direction of the cross-dispersion, and it is possible that the grism was not well secured, flopping between two positions. Figure 1 shows the position of the spectrum on the chip as a function of telescope hour angle, from which it is clear that the flop occurs near the meridian. To account for the shift in the data reduction, each spectrum and its associated calibration spectrum was classified into a “high” or “low” group. Separate flats and high-order wavelength calibrations were made for each group and the associated frames were reduced within its group. Three frames that suffered a shift during an exposure were discarded.

A velocity for each spectrum was calculated relative to a high signal-to-noise spectrum of the star HD 83443 using the Fourier quotient technique of Sargent *et al.* (1977). Several of the Cepheid candidates were too heavily reddened to provide an adequate signal for radial velocities using the blue orders, so we decided to use the Ca triplet (8498, 8542, 8662 Å) in order 14 to measure individual velocities. Several CORAVEL faint southern radial velocity standards (Maurice *et al.* 1984) were observed throughout the run, and were used to calibrate the effective velocity of the template spectrum. The individual measurements of the standards (given as an effective template velocity, computed using radial velocity of the standard star, as by Metzger *et al.* 1991) are shown in Figure 2. The open and filled points correspond to “low” and “high” position spectra, respectively. The mean template velocities of the two groups are not significantly different, confirming that the two groups of spectra have been successfully referenced to the same zero point. Table 1 shows the mean measured velocities for each radial velocity standard, along with velocities for two metal-weak subdwarfs observed during the run. Each velocity has been adjusted upward by  $0.4 \text{ km s}^{-1}$  to bring these velocities to a minor planet-based zero point (Mayor 1985; Metzger, Caldwell, & Schechter 1992, hereafter MCS). Two error estimates are given in Table 1:  $\varepsilon_f$ , the formal error in the velocity from the Fourier quotient, and  $\varepsilon_V \equiv \sigma_v/\sqrt{n}$ , the standard error of the mean of the individual measurements.

The individual radial velocities for the stars confirmed as Cepheids are given in Table 2. The other variables did not have spectra consistent with that of a Cepheid; most of these did not have significant Ca triplet absorption lines and thus did not yield radial velocities.

## 2.2. Gamma Velocities

Gamma velocities were computed for each of the Cepheids according to the method described by MCS. For each star, the radial velocity points are folded at the pulsation period and fit to a

“typical” radial velocity curve. The shape of this velocity curve is fixed by the photometrically determined period of the Cepheid, and is generated using low-order Fourier coefficients that are functions of the period. The periods used for these stars were taken from Avruch (1991), and improved with additional data below. The gamma velocity and phase are then fit using a  $\chi^2$  minimization procedure.

The radial velocities for each star and the curves fit to the points are shown in Figure 3. Fit gamma velocities for the eight Cepheids are given in Table 3, along with the formal error of the fit and the reduced  $\chi^2$ . An additional error estimate, based on a Monte Carlo simulation, is also given in Table 3. This estimate takes the variation in the shape of the fit curve into account as well as velocity measurement error. One star thought to be a Cepheid from its light curve (11582-6204), but suspect due to its near-infrared photometry (Schechter *et al.* 1992), has a spectrum inconsistent with that of a Cepheid and was discarded from the candidate list.

### 2.3. Infrared Magnitudes

Mean  $\langle K \rangle$  magnitudes of the new Cepheids were computed using the data of Schechter *et al.* (1992). The values of  $\overline{K}$  they report are a straight average of their individual measurements; if the measured points are not well-spaced in phase, such an average can be biased with respect to the true  $\langle K \rangle$ . Though we expect this difference to be small given the pulsation amplitude at  $K$ , to obtain a slightly more accurate average we fitted a sine function to the  $K$  points using periods computed above. The amplitude of the sine function was scaled from the  $V$  light curve amplitude, computed from the data of Avruch (1991) and LeDell (1993), using the relation of Welch *et al.* (1984):  $\text{Amp}(K) = (0.30 \pm 0.03) \times \text{Amp}(V)$ . The results of this procedure, along with formal errors assuming  $\sigma_K = 0.02$  mag for each observation, are given in Table 4. Adding higher-order terms to the light curves from the Fourier decompositions of Laney & Stobie (1993a) had no significant effect on the computed  $\langle K \rangle$ . The star 13240–6245 has a high covariance ( $r \simeq 0.6$ ) between  $\langle K \rangle$  and the epoch, largely a result of poor phase coverage.

Also shown in Table 4 are the amplitudes (peak-to-peak) of the  $V$ -band light curves, epochs of maximum light in both  $V$  and  $K$ , and improved period estimates. The  $K$ -band epochs were determined from the fit light curve, and the improved periods are selected from values listed by Avruch (1991) (he gives several due to the possibility of aliasing) that are most consistent with the  $K$  data. We find that the  $V$  maximum light lags that in  $K$  by  $\sim 0.27$  cycles, in rough agreement with Welch *et al.* (1984). We also note that the star 13323–6224 is peculiar in that it has a significantly smaller amplitude than expected given its period. Overall, we obtain a tight formal error on the  $\langle K \rangle$  magnitudes; in particular, the uncertainties are smaller than the scatter in the PL- $K$  relation and hence sufficient for our purposes. (It is interesting to note that only two of the average magnitudes are significantly different from the straight means computed by Schechter *et al.* [1992].) It was not necessary to phase and fit the  $(H - K)$  colors, since they do not change appreciably over the pulsation cycle.

We used the  $E(H - K)$  color excesses of Schechter *et al.* (1992) to compute the extinction in  $K$ ,  $A_K \equiv K - K_0$ , for the newly discovered Cepheids. These were derived assuming an intrinsic color locus in the H–K/P plane:  $(H - K)_0 = 0.068 + 0.024(\log P - 1)$  (their equation 1). We adopted the same extinction law used by Schechter *et al.* for the total-to-selective extinction, that given by Cohen *et al.* (1981):  $A_K = 1.39E(H - K)$ . This can be compared with coefficients found in other sources: 1.7 (McGonegal *et al.* 1983, CIT system), 1.5 (Clayton, Cardelli, & Mathis 1989, Johnson system), 1.8 (Rieke & Lebofsky 1985), and 1.6 (Laney & Stobie 1993a, Carter system). The Caldwell *et al.* Cepheids have an average  $E(H - K)$  of 0.27; if we were to simply replace our reddening law with the average of the  $A_K/E(H - K)$  values listed (= 1.6), the result would be an increase in mean distance modulus by 0.06 mag for the stars in the sample. This would not be strictly correct, however, as the values are based on magnitudes of different systems; we use the Cohen *et al.* (1981) value, keeping in mind a possible systematic offset.

### 3. Galactic Cepheid Data

The new Cepheid data from §2 were combined with a catalog of Cepheid photometry and radial velocities compiled from several sources. We started with the compilation of 184 stars by CC. Reddenings for many additional Cepheids were obtained from Fernie (1990, 1994), and new radial velocities from Moffett & Barnes (1987), Mermilliod *et al.* (1987), and MCS. Finally, mean B and V photometry and many new radial velocities were obtained from the compilation of PMB. Known or suspected W Virginis stars (Pop. II Cepheids), based on the list of Harris (1985), were excluded from the sample.

Because of the small scale height of Cepheids in the Galactic disk, the distant stars lie within a few degrees of the Galactic plane in projection and are thus significantly obscured by dust. To measure distances, accurate color excesses for the stars must be known to allow an estimate of the total extinction. Figure 4a shows a comparison between the color excess given by CC and the values of Fernie (1990). A clear trend is evident, such that the redder stars tend to have higher values of  $E(B-V)$  on Fernie’s scale than that of CC. A linear fit to the data gives

$$E_{B-V}(\text{CC}) - E_{B-V}(\text{F90}) = 0.032(\pm 0.006) - 0.107(\pm 0.013) \times E_{B-V}(\text{F90}), \quad (1)$$

with a 0.05 mag scatter about the fit. This trend implies a difference in  $R \equiv A_V/E(B - V)$  between the two systems of 10%, or about 0.3 mag in the corrected  $V$  magnitude for the more heavily extinguished stars ( $E_B - V \simeq 1$ ). The origin of the discrepancy is not clear, but it is significant: a 10% change in  $R$  corresponds to a 5% change in  $R_0$  derived from rotation curve models (see §4 below). A comparison between reddenings of Fernie (1990) and Dean, Warren, & Cousins (1978) for 94 stars in common, yields a similar but shallower slope; Fernie shows a similar plot for cluster stars in his Figure 1. Another comparison can be made to the recent study of Cepheid reddenings by Laney & Stobie (1994), who combined optical and infrared data to test the value of  $R$ . Figure 4b shows a comparison of their reddenings to Fernie’s, revealing the same trend

as Figure 4a. We have adopted the same value of  $R$  as Laney & Stobie found consistent with their color excesses, thus to produce extinction corrections we adjust Fernie’s (1990) reddenings using equation 1.

The combined data set contains 294 stars (not including the eight new stars from §2) and is shown in Table 5. Values reported for  $E(B-V)$  are primarily from Fernie (1990), transformed to our system.

### 3.1. Cepheid Distance Calibration

Distances to the Cepheids were computed primarily via the period-luminosity relation in the V-band (PL-V), which can be parameterized

$$5 \log_{10} d = m - m_0 - \alpha(\log P - 1). \quad (2)$$

Here  $m_0$  corresponds to the unreddened apparent magnitude of a Cepheid with a 10-day period at a distance of  $R_0$ , and  $\alpha$  is the slope of the adopted period-luminosity relation. The measured period and unreddened apparent magnitude for a particular Cepheid are given by  $P$  and  $m$ , respectively. The stars were dereddened as in CC, using the prescription for  $R_V$  derived from Olson (1975) and Turner (1976):

$$R_V \equiv A_V/E(B - V) = 3.07 + 0.28(B - V)_0 + 0.04E(B - V),$$

whereby

$$m = \langle V \rangle - R_V \times E(B - V).$$

This extinction correction is also used by Laney & Stobie (1993), and has a slightly higher value for the effective  $R_V$  than the reddening laws of Savage & Mathis (1979) and Rieke & Lebofsky (1985) (though the last two do not give an explicit dependence on intrinsic color). The dependence of  $R_V$  on the intrinsic color is caused by a shift in effective wavelength of the filters when measuring stars of different spectral class (Olson 1975). Extinction corrections for infrared photometry are handled separately and are described below.

We chose to avoid period-luminosity-color (PLC) relations and terms accounting for metallicity in this study for two reasons. First, the PL-V relation is thought to be only weakly sensitive to metallicity, both in zero-point and slope (Iben & Renzini 1984, Freedman & Madore 1990; but see also Caldwell & Coulson 1986), and less sensitive to metallicity than the PLC relation (Stothers 1988). Second, the intrinsic color used in the the PLC relation is susceptible to significant error when this color is found by dereddening using color excesses. By making a correction based on color, one must make some implicit assumption about the intrinsic color of the star; any difference between this assumption and the actual color (perhaps due to metallicity) is amplified in the derived unreddened magnitude. This process can significantly increase the sensitivity of PLC

distances to metallicity. The uncertainties in the reddening corrections themselves tend to be larger than the effect of metallicity on the PL-V relation over a wide range of metal abundance (Stothers 1988). Further, the reddenings derived for Cepheids themselves are sometimes derived under the assumption of a unique color locus in the (B–V)/(V–I) plane (e.g. Dean, Warren, & Cousins 1978). Given these sources of error, and the uncertainty in the slope of the PLC color term (Fernie & McGonegal 1983, Caldwell & Coulson 1986), for this study we chose to use only PL relations (PL-V, plus the PL-K relation for some of the models below) with no explicit correction for a radial metallicity gradient. The scatter in the individual distances may be slightly higher, but the systematic errors are easier to quantify.

The two parameters  $m_0$  and  $\alpha$  in equation 2 determine the distances to each Cepheid in terms of  $R_0$ . The PL-V slope parameter  $\alpha$  has been measured using both Magellanic Cloud and Galactic cluster Cepheids (Fernie & McGonegal 1983, Caldwell & Coulson 1986, CC, Madore & Freedman 1991, Laney & Stobie 1994). Most tend to agree to within the quoted errors, and lie in the range  $-2.9$  to  $-2.8$  (with the exception of CC at  $-3.1$ ). There does appear to be a significant difference in computed slope of the PL relation, however, depending on the period range of Cepheids used in the fit. While studies using open clusters to calibrate the PL relation contain data over a wide range of period, many exclude the longest period Cepheids from the fit as they tend to be somewhat brighter than an extrapolation of the PL relation of short-period Cepheids would indicate (e.g. Fernie & McGonegal 1983). Freedman *et al.* 1993 derive a separate calibration of the PL relation based only on Cepheids with  $1.0 < \log P < 1.8$  to match most closely the range of periods in the M81 Cepheids. They find a PL-V slope of  $-3.35 \pm 0.22$ , significantly steeper than when short-period Cepheids are used.

A possible explanation for the discrepancy is the suggestion by Böhm-Vitense (1994) that most Cepheids with periods shorter than 9 days are overtone pulsators. If the short and long period Cepheids form two offset, steeper PL relations, then a slope measured from combining the two would be shallower than that measured from either set independently. More work needs to be done to help verify the existence of the separate PL relations, particularly in the near-infrared where the intrinsic scatter about the PL relation is smaller. A quick examination of the PL-K data of Laney & Stobie (1994) shows little evidence for short-period overtone pulsators, while not necessarily ruling them out. Gieren, Barnes, & Moffett (1989) find evidence against this hypothesis based on the continuity of BW radii across a wide range of periods.

There is direct evidence, however, that at least some of the Cepheids in our sample are overtone pulsators. For example, the recently measured radial velocities for QZ Nor of  $-38.6 \pm 0.7$  km s<sup>-1</sup> (MCS) and V340 Nor of  $-40.0 \pm 0.1$  km s<sup>-1</sup> (Mermilliod *et al.* 1987) confirm both as members of NGC 6067, and support the conclusion of Coulson & Caldwell (1985) and Moffett & Barnes (1986) that QZ Nor is an overtone pulsator while V340 Nor is not. Given this conclusion, the period-luminosity relation gives the same distance to both. Other examples of such direct evidence include SU Cas (Evans 1991).



Even with some contamination from overtone pulsators, so long as the range of periods of the calibrators is similar to the overall population, the derived slope and zero-point will still provide accurate distances (though perhaps with larger scatter). Considering that our Cepheid sample has a median  $\log P \approx 0.9$ , we can comfortably use the shallower slopes derived from Cepheids of similar period, and adopt a commensurate zero point. New data on Magellanic Cloud Cepheids discovered in the MACHO survey (Alves *et al.* 1995, Alcock *et al.* 1995) will help to answer this question conclusively.

The zero point of the Cepheid PL relation puts  $m_0$ , the unreddened apparent magnitude of a Cepheid at a distance  $R_0$ , on an absolute distance scale. Various studies have yielded different Cepheid PL zero points, primarily due to differences in assumed extinction, metallicity or correction for metallicity, and the sample of stars used. Currently the most accurate methods for Galactic PL calibrations are those using Cepheids in clusters and associations (Turner 1985; Fernie & McGonegal 1983), and those using the visual surface brightness (Baade-Wesselink) method (Gieren, Barnes, & Moffett 1989). The cluster calibrations are based on fitting main sequences for clusters containing Cepheids to either the Hyades or Pleiades, and the surface brightness method attempts to measure the radius of a Cepheid based upon accurate photometry and radial velocity measurements. A convenient comparison of Cepheid calibrations can be made by applying the calibrations to LMC Cepheids, and comparing the derived LMC distance moduli. The SMC is somewhat less suited to this purpose as it is thought to be significantly extended along the line of sight. Feast & Walker (1987) give a comprehensive review of Cepheid calibrations up to that time, and conclude that for a Pleiades modulus of 5.57, the LMC lies at a true distance modulus of  $18.47 \pm 0.15$ . This estimate is based on the same extinction law used here. More recently, using updated V-band data, CC determine an LMC modulus of 18.45, and Laney & Stobie (1994) find  $18.50 \pm 0.07$ , both assuming the same Pleiades modulus and extinction law. The visual surface brightness calibrations currently yield Cepheid distance moduli larger by  $\sim 0.15$  mag on average (Gieren & Fouqué 1993), and give a distance modulus for the LMC of  $18.71 \pm 0.10$  mag. While significantly different, the Gieren & Fouqué data appear to have an asymmetric distribution that may make the distance moduli too large: the four calibrators they discard as being significantly discrepant all have distance moduli too large by  $> 0.6$  mag. Though this does not completely resolve the discrepancy, for this study we have chosen to adopt the cluster calibrations. On this scale, our adopted V-band calibration is

$$M_V = -4.10 - 2.87(\log P - 1). \quad (3)$$

The internal uncertainty in the zero point (exclusive of any systematic error in the Pleiades/LMC distance) is estimated to be  $\simeq 0.07$  mag.

To incorporate the near-infrared data on the newly-discovered Cepheids, we use the period-luminosity relation in the  $K$ -band with an appropriate calibration and extinction law. The calibration zero point must give distances commensurate with those derived from  $V$ -band data, and thus we again normalize the zero-point to an LMC modulus of 18.50. After making this correction, the PL- $K$  calibration of Welch *et al.* (1987) gives  $M_K = -5.66 - 3.37(\log P - 1)$ ,

with the  $K$  magnitudes on the same system (Elias *et al.* 1982) as the Schechter *et al.* (1992) photometry. Madore & Freedman (1991) give a self-consistent calibration based on a sample of 25 LMC Cepheids, each with photometry in both  $V$  and  $K$ , finding  $M_K = -5.70 - 3.42(\log P - 1)$ , identical to within quoted errors. The Madore & Freedman PL- $V$  calibration is also consistent with our adopted  $M_V$ . Laney & Stobie (1994) give a calibration of the PL- $K$  relation in a slightly different photometric system; after converting to the Elias *et al.* (1982) system using the transformation of Laney & Stobie (1993b), and adjusting to an LMC modulus of 18.50, we find

$$M_K = -5.70(\pm 0.04) - 3.40(\pm 0.05)(\log P - 1). \quad (4)$$

The scatter of the individual stars about the period-luminosity relation is significantly smaller in  $K$  than  $V$ , 0.16 mag rms vs. 0.25 mag rms, and hence the internal error associated with the zero point is correspondingly smaller at 0.04 mag. Since the quoted uncertainties in the Laney & Stobie (1994) calibration are the smallest of those quoted above, and that the relation is almost identical to the others, we adopt equation 4 for our models.

There is a small discrepancy between the LMC moduli derived from  $V$  and  $K$  data when using Galactic cluster calibrations. Measurements of LMC distance modulus in the  $K$  band from the above references typically yield a value of 18.55–18.60, some 0.05–0.10 higher than the  $V$  calibration. This discrepancy could be due to a number of factors, including a difference in mean metallicity between Galactic and LMC Cepheids. As the bolometric PL relation for Cepheids is thought to be essentially independent of metallicity (Iben & Renzini 1984), the zero point of the PL- $V$  and PL- $K$  relations may be expected to differ by  $\sim 0.03$  mag over the metallicity difference of the Galaxy and the LMC from the variation in bolometric correction alone (Laney & Stobie 1994, Stothers 1988). Another possible source of systematic error arises from the correction for extinction: this is substantially larger for the Galactic calibrators, which have a mean  $E(B-V)$  of 0.65 (Feast & Walker 1987), than the LMC Cepheids, which have an  $E(B-V)$  of about 0.14 mag. A reasonable error of 0.1 in the adopted  $R_V$  value would thus produce an apparent distance offset between the two of 0.05 mag. Since the difference here is only slightly greater than  $1 \sigma$ , no useful limits can be placed on  $R$  (or  $A_V - A_K$ ). However, we discuss below some implications of the kinematic distance scale using the newly discovered Cepheids on the adopted reddening law.

#### 4. Milky Way Rotation

Figure 5 shows a geometric picture of a star with angular velocity  $\Theta$  at a distance  $D$  from the Sun, and at a distance  $R_0$  from the center of the galaxy. The local standard of rest (LSR) rotates with velocity  $\Theta_0$ , and the Sun moves with a velocity peculiar to the LSR of  $(u_0, v_0, w_0)$  in the coordinates  $(R, \Theta, Z)$ . For our models we assume that the height above the disk,  $|z| = D|\sin b|$ , is sufficiently small that the potential is dominated by the disk, and therefore a thin-disk model adequately represents the orbits (i.e. the primarily rotational orbits of the stars are decoupled from their vertical motion). This condition is met by the classical Cepheid population as they

are confined to the disk with a scale height of 70 pc (average absolute distance from the mean plane, Kraft & Schmidt 1963). We also fix the  $Z$ -component of the Sun’s motion,  $w_0$ , at  $7 \text{ km s}^{-1}$  (Delhaye 1965) as it is neither constrained by the data nor does it affect the model.

The rotation models we employ take the form of a mean velocity field  $\Theta(R, \phi)$  with components in the  $\hat{R}$  and  $\hat{\phi}$  directions. The mean velocity of the stars at  $(R, \phi)$ , as measured from the Sun, is

$$v_r^* = \Theta_R(R_0, 0) \cos \ell \cos b - \Theta_R(R, \phi) \cos(\phi + \ell) \cos b - \Theta_\phi(R_0, 0) \sin \ell \cos b + \Theta_\phi(R, \phi) \sin(\phi + \ell) \cos b - v_{\odot*}. \quad (5)$$

The Sun’s peculiar motion relative to the LSR in the direction of the star,  $v_{\odot*}$ , is given by

$$v_{\odot*} = -u_0 \cos \ell \cos b + v_0 \sin \ell \cos b - w_0 \sin b. \quad (6)$$

The data are fit to the models using a non-linear  $\chi^2$  minimization program. Free parameters were determined by fitting the measured radial velocities for each Cepheid to model velocities generated from the other measured quantities ( $\ell$ ,  $b$ ,  $\langle V \rangle$ ,  $P$ , and  $E(B - V)$ ) via equation 5. Each measured velocity was weighted as in CC using the estimated radial velocity dispersion added in quadrature to the effective velocity error introduced by the distance measurement:

$$\sigma_i^2 = \sigma_v^2 + \sigma_d^2 (\partial v_r / \partial d)^2. \quad (7)$$

The dispersion in the radial velocities is a combination of measurement error and the intrinsic velocity dispersion of the stars in the disk (the latter dominating), and was taken to be  $\sigma_v = 11 \text{ km s}^{-1}$ . The random error in the distance from all sources (measurement, extinction correction, and PL dispersion),  $\sigma_d$ , was assumed to be 0.2 mag.

#### 4.1. Axisymmetric Models

The initial models we use to derive parameters of Galactic rotation are based on a linear, axisymmetric rotation curve in a manner similar to CC. An axisymmetric rotation curve is given by  $\Theta_R = 0$  and  $\Theta_\phi(R)$  independent of  $\phi$ . If we make the approximation that the rotation curve is linear, i.e. that

$$\Theta_\phi(R) \approx \Theta_0 + (R - R_0) \left( \frac{d\Theta}{dR} \right)_{R_0} = \Theta_0 + (r - 1) \left( \frac{d\Theta}{dr} \right)_{r=1},$$

equation 5 reduces to (cf. Mihalas & Binney 1981, CC)

$$v_r^* = -2AR_0 \left( 1 - \frac{1}{r} \right) \sin \ell \cos b - v_{\odot*}. \quad (8)$$

Here we have defined  $r \equiv R/R_0$ , and  $A$  is Oort’s constant

$$A \equiv \frac{1}{2} \left[ \frac{\Theta_0}{R_0} - \left( \frac{d\Theta}{dR} \right)_{R_0} \right].$$

The transformation of the heliocentric distance  $d \equiv D/R_0$  to the Galactocentric distance  $r$  is given by

$$r^2 = 1 + d^2 - 2d \cos \ell. \quad (9)$$

While the expansion of the rotation curve is to first order in  $r$ , and thus is valid primarily for stars near the solar circle, no approximation is made for small  $d$ .

An additional parameter was added to compensate for a possible zero-point offset in the radial velocities ( $\delta v_r$ ). The full model for the measured heliocentric radial velocity of a star is then

$$\begin{aligned} v_r = & -2AR_0 \left( 1 - \frac{1}{r} \right) \sin \ell \cos b \\ & + u_0 \cos \ell \cos b \\ & - v_0 \sin \ell \cos b \\ & - w_0 \sin b - \delta v_r. \end{aligned} \quad (10)$$

Note that the sign of  $u_0$  follows a Galactic radial convention and is opposite that used by CC. The model has parameters  $2AR_0$ ,  $m_0$ ,  $\alpha$ ,  $u_0$ ,  $v_0$ ,  $w_0$ , and  $\delta v_r$ ;  $\alpha$  was fixed according to the PL relation adopted,  $w_0$  was fixed as described above, and the remaining parameters were fit using the  $\chi^2$  minimization routine.

Table 6 gives a summary of the results of the axisymmetric models. Model A1 includes all of the sample Cepheids, including the 8 new Cepheids with distances determined from K-band photometry and reddenings. Distances to the remaining stars were computed using the color excess scale given by equation 1. Model A1.1 is identical except for the exclusion of 6 stars with large residuals in model A1: FF Car, FM Car, BB Gem, VW Pup, AA Ser, and V Vel. The model parameters remain essentially the same, while the associated uncertainties fall (the six excluded stars contribute almost 25% of the residual error in model A1). The error on  $R_0$  and  $2AR_0$  are independently less than 5%; the high covariance of the two errors (see below) implies an even tighter constraint on  $A = 2AR_0/2R_0 = 15.4 \pm 0.3 \text{ km s}^{-1} \text{ kpc}^{-1}$ . It is important to note that the errors given are internal errors (those due to scatter about the adjustable parameters), and do not include systematic uncertainties associated with the fixed model. Model A1.2 uses the same stars as A1.1, but employs the color excesses of Fernie (1990) directly, without adjustment. The most significant effect is a shortening of the distance scale by  $\sim 5\%$ .

As a check, we ran our modeling software on the data used by CC in their study. The parameters are listed as model A2 in Table 6, and agree well with those determined by CC. The largest difference between the A1 and A2 parameters, aside from the reduced uncertainties, is the value determined for  $2AR_0$ . Model A2.3 was run on the same set of Cepheids, but with updated

velocities from Table 5 and reddenings from Fernie (1990). Again,  $m_0$  decreases by about 5%, while  $2AR_0$  increases by  $0.8\sigma$ . Oort’s  $A$  constant effectively increases from  $14.2 \text{ km s}^{-1} \text{ kpc}^{-1}$  to  $15.7 \text{ km s}^{-1} \text{ kpc}^{-1}$  when the new data are used. Models A2.2 and A2.3 show the effect of adding the new velocities and reddenings separately.

We also fit our models to the data set used by PMB as a further test. Model A3 uses their pruned set of 266 stars, and further the parameter  $\delta v_r$  was fixed at zero as in their study. Our model reproduces their results closely, though our estimates of uncertainty in the model parameters are somewhat larger than reported by PMB.

Since the PMB study employed color excesses on the F90 scale, the effective distance scale should be the same between model A3 and A1.2. However, the computed  $R_0$  is somewhat larger in model A3 than A1.2, indicating a difference in the implied distance to the Galactic center. At first we guessed this might be due to the effect of adding the eight new distant Cepheids to the model—the high leverage on  $R_0$  for these stars could produce the change (particularly since distances were computed using a separate PL relation). Deleting these stars, however, only increased the uncertainty of  $R_0$  without changing the most likely value. We found that the discrepancy was caused by including the  $\delta v_r$  parameter in the model: the values determined for  $R_0$  and  $2AR_0$  fall by  $1\text{-}\sigma$  (model A3.1 vs. model A3), and resolve the discrepancy. We conclude that not including the  $\delta v_r$  in the axisymmetric models skews PMB’s  $R_0$  measurement slightly high. Allowance for this term can be made in non-axisymmetric models, as PMB suggest, and is treated in §4.2.

We can further determine the effect of the new Cepheid data by examining the covariances between model parameters. Table 7 shows the covariances of the model parameters determined using different sets of data. Covariances are expressed here as correlation coefficients of the projected data (Bevington 1969):

$$r_{ij} = \frac{s_{ij}^2}{s_{ii}s_{jj}}$$

where the  $s_{ij}^2$  are elements of the covariance matrix. The reduction in the covariance between  $m_0$  and  $2AR_0$  in the model including the new Cepheids (A1.1) over that without (A1.4) is due to the advantageous placement of the new Cepheids. Because they lie at a Galactocentric radius near the solar circle, the mean radial velocity of the stars in the model is close to zero, independent of rotation speed. (In an axisymmetric model, stars lying at the same radius rotate together in a ring with no relative velocity, save for random motion.) Thus adding only a few stars serves to decouple the two parameters in the model. Figure 7 shows a comparison between constant  $\chi^2$  contours in  $m_0$ ,  $2AR_0$  space with and without the eight stars.

The eight new CKS Cepheids turn out to provide a useful constraint on  $R_0$  by themselves, assuming axisymmetric rotation. Fitting the eight Cepheids to the model, we derive  $R_0 = 8.1 \pm 0.5 \text{ kpc}$ , assuming  $v_0 = 14 \text{ km s}^{-1}$ . Thus with just eight stars, knowing  $v_0$  gives us a distance to the Galactic center to 6% precision. If we remove the nearest Cepheid, 13323-6224 at  $0.3R_0$ , most of

the remaining covariance between  $R_0$  and  $2AR_0$  is eliminated. The error reduces to  $\sim 4\%$ , with  $R_0 = 7.95 \pm 0.31$  kpc. The parameters  $R_0, v_0$  have a high covariance in this model; decreasing  $v_0$  by  $4 \text{ km s}^{-1}$  reduces the derived value of  $R_0$  by 5%. Again, all of these models rely on the assumption of an axisymmetric rotation curve; in the next section, we relax this assumption.

## 4.2. Non-Axisymmetric Models

The persistence of a significant  $\delta v_r$  in the Cepheid data, even after significant improvements in radial velocities and distances, leads to the conclusion that either some systematic error is present in measuring  $\gamma$ -velocities of Cepheids, or that an axisymmetric model is not sufficient to describe the rotation curve. As many Cepheids in open clusters now have accurate  $\gamma$ -velocities within  $0.4 \text{ km s}^{-1}$  of the cluster mean velocity (e.g. Mermilliod *et al.* 1987), the systematic error in measuring  $\gamma$  is probably small. Based on a comparison with an N-body simulation, PMB suggest that the effect could be due to non-axisymmetric motion driven by a central bar of  $\sim 5$  kpc in extent. Here we examine the shape of the local rotation ellipticity directly using a simple non-axisymmetric model.

Our non-axisymmetric models are based on those of Kuijken & Tremaine (1994, hereafter KT). The rotation curve is produced by a primarily axisymmetric potential with a small  $m = 2$  perturbation, with minor axis in the direction  $\phi_b$ . The circular velocity and potential ellipticity have a power-law dependence on radius:

$$v_c(R) = \Theta_0 \left( \frac{R}{R_0} \right)^\alpha ; \quad \epsilon(R) = \epsilon_0 \left( \frac{R}{R_0} \right)^{p-2\alpha}. \quad (11)$$

The rotation curve is given by equation (5) and by (KT, eqn. 5a):

$$\begin{aligned} \Theta_R(R, \phi) &= \beta_1 v_c(R) [s(R) \cos 2\phi - c(R) \sin 2\phi], \\ \Theta_\phi(R, \phi) &= v_c(R) - \beta_2 v_c(R) [c(R) \cos 2\phi - s(R) \sin 2\phi], \end{aligned} \quad (12)$$

where we have defined

$$\beta_1 \equiv \left( \frac{1 + p/2}{1 - \alpha} \right), \quad \beta_2 \equiv \left( \frac{1 + p(1 + \alpha)/4}{1 - \alpha} \right) \quad (13)$$

and two orthogonal projections of the ellipticity

$$c(R) \equiv \epsilon(R) \cos 2\phi_b, \quad s(R) \equiv \epsilon(R) \sin 2\phi_b. \quad (14)$$

The  $c(R)$  and  $s(R)$  parameters correspond to components of the ellipticity that are symmetric and antisymmetric, respectively, about the Sun-center line  $\phi = 0$ .

As pointed out by KT, if the Sun lies near a symmetry axis of a non-axisymmetric distortion, it is not easily detected using data such as our sample where  $d \lesssim R_0$ . In particular, the parameters  $c$  and  $R_0$  in the models have a high covariance, and thus do not produce independent information.

If such a distortion were present ( $c$  non-zero), the derived parameters  $R_0$  and  $2AR_0$  can deviate significantly from their true values. To judge the size of the effect for our data, we have fit a simple model with a flat rotation curve and constant ellipticity ( $p = \alpha = 0$ ), and allow the symmetric ellipticity component  $c$  to vary along with the other parameters. For this model, the predicted mean radial velocities reduce to

$$v_r = \Theta_0 \left( \frac{1}{r} - 1 \right) \sin \ell \cos b + \frac{\Theta_0}{r} c (2d \cos \ell - 1) \sin \ell - v_{\odot*} . \quad (15)$$

As expected, if we fit for all six parameters, we find a covariance between  $2AR_0$ ,  $m_0$ , and  $c$  of 0.95—too large to make any independent constraints on these parameters. We can, however, fix the symmetric ellipticity in the models and determine how this affects the other derived parameters. Figure 8 shows how  $m_0$  and  $2AR_0$  vary as a function of the ellipticity parameter. From a combination of non-kinematic estimates of  $R_0$  (Reid 1993), we can deduce a weak constraint on the ellipticity at the solar circle  $-0.08 < c(R_0) < 0.14$ .

Because  $c$  is degenerate with other parameters, we fix it at zero and investigate the antisymmetric term  $s$ . For these models we incorporate the same data set used in model A1.1, and for the primary model assume a flat rotation curve and constant ellipticity ( $\alpha = p = 0$ ). Here we also assume that the velocity offset  $\delta v_r$  is a kinematic effect of the other model parameters, and therefore fix  $\delta v_r = 0$ . Table 8 shows the results of several models. Model B1 gives results for the primary elliptical model, and shows a  $2.5\sigma$  detection of ellipticity,  $s(R_0) = 0.043 \pm 0.016$ . The B2 models vary the extinction coefficient  $R$ , and B3 models vary  $p$  and  $\alpha$ ; the ellipticity detection is robust in all except the  $p > 0$  models. Note that while the implied circular velocity increases rapidly as  $\alpha$  increases, Oort’s A remains roughly constant. Velocity residuals for model B1 are shown in Figure 9; there is some hint that systematic velocity structure not accounted for by the simple models is present, perhaps due to the influence of spiral structure.

## 5. Discussion

The uncertainties quoted in Tables 6–8 correspond to internal error estimates in the models, derived from the scatter of the data about the fit model. As described in §3.1 above, systematic uncertainties in the distance scale are also present. To summarize, the internal uncertainty in the  $V$ -band zero point is  $\simeq 0.07$  mag, to which we add an estimated 0.1 mag error in the Pleiades modulus; similarly, the internal uncertainty in the  $K$ -band calibration is 0.04 mag. Thus we adopt a calibration error of 0.12 mag and 0.11 mag for  $V$  and  $K$  zero points, respectively. There is also an uncertainty associated with the reddening scale for the  $V$ -band distances; however, we note that since we have a good measurement of  $R_0$  based only on  $K$ -band photometry, this uncertainty does not contribute to the overall distance scale error. The reddening uncertainty in the  $K$ -band corresponds to  $\sim 0.05$  mag in  $R_0$ . The  $K$ -band distance scale agrees closely with that derived

from the full models using the Dean *et al.* (1978) optical reddening scale, thus we adopt that scale for our derived distances. The largest systematic uncertainty in measuring  $R_0$ , however, derives from the inability of the rotation models to adequately constrain  $c(R_0)$ . KT suggest, based on a combination of local kinematics and global HI distribution, that  $c(R_0) = 0.082 \pm 0.014$ . This corresponds to overestimating  $R_0$  in the kinematic models by  $\sim 15\%$  (see Figure 8). For now, we keep this component of the systematic uncertainty separate; below we see that based on the RR Lyrae distance scale,  $c(R_0)$  is likely small. Our standard model B1 then gives  $R_0 = 7.66 \pm 0.32 \pm 0.44$  kpc and  $v_c(R_0) = 237 \pm 12 \pm 13$  km s $^{-1}$ . Computing Oort’s A from these gives  $A = 15.5 \pm 0.4 \pm 1.2$  km s $^{-1}$  kpc $^{-1}$ .

Since the models of CC, the number of Cepheids with data adequate for use in rotation models has increased by 50%, in particular the addition of stars at large distance from the Sun that provide good leverage for measuring scale and shape parameters. The internal uncertainty in  $R_0$  and  $2AR_0$  has decreased by approximately a factor of two, while remaining consistent in their mean values. In comparison with the recent PMB models, our measurement of  $R_0$  is slightly smaller than that found by PMB, 8.1 kpc; much of this difference can be attributed to the absence of a direct ellipticity term in the PMB models. This also appears to skew the measurement of  $2AR_0$  to the high side; our derived values differ by almost  $2\text{-}\sigma$ . We find that other differences between our models, including a higher-order expansion of the rotation speed and a different minimization algorithm, produce negligible differences in the fit parameters.

Our results compare favorably with other methods of determining  $R_0$ . Reid (1993) computes a “best value” for  $R_0$ , based on a weighted average of many techniques, of  $8.0 \pm 0.5$  kpc, in agreement with the results from this paper. In particular, Reid divides measurements into several categories; our present results fall into two different categories, one that is based primarily on the calibration of the  $K$ -band Cepheid PL relation, and one that is based on a kinematic rotation model. Our distance is somewhat larger than that implied by a direct measurement of the distance to Sgr B2 at the Galactic center of  $7.1 \pm 1.5$  kpc (Reid *et al.* 1988), though still well within the errors. A direct measurement of the proper motion of Sgr A\* by Backer & Sramek (1987), when interpreted with our measured circular velocity, translates to  $8.3 \pm 1.0$  kpc, again consistent with our measurement, though the uncertainty is a factor of 2–3 larger.

We can also use  $R_0$  as a standard length to compare the Cepheid and RR Lyrae distance scales. Based on new near-infrared photometry of RR Lyraes in Baade’s window, Carney *et al.* (1995) measure  $R_0$  to a precision of about 5%. This result is much less sensitive to the uncertain extinction correction than the previous optical work (e.g. Walker & Terndrup 1991), and is also independent of the rotation curve shape. Carney *et al.* quote two different values for  $R_0$ :  $7.8 \pm 0.4$  kpc, based on the zero-point calibration of Carney, Storm, & Jones (1992, CSJ); and  $8.9 \pm 0.5$  kpc, based on an RR Lyrae calibration from the LMC corresponding to an LMC modulus of 18.50. As noted by Walker (1992), the Cepheid LMC distance modulus is 0.2–0.3 mag higher than that derived from LMC RR Lyraes on the CSJ zero point. Our result for  $R_0$  agrees quite well with the CSJ-scale distance, and is about  $2\text{-}\sigma$  below the LMC RR Lyrae-based calibration. The systematic



change in our  $R_0$  measurement implied by increasing  $c(R_0)$  is in the opposite sense to that implied by adopting an LMC RR Lyrae distance modulus of 18.50: if the KT suggestion that  $c(R_0) \simeq 0.08$  is correct, it would only make our estimate for  $R_0$  shorter and the discrepancy with the LMC RR Lyrae calibration larger. Thus the CSJ calibration of RR Lyraes and the Cepheid distance scale appear to be commensurate to within  $\sim 0.15$  mag, and the ellipticity term  $c(R_0) < 0.04$ . This implies that a small but probably real discrepancy exists between Cepheid and RR Lyrae LMC distances, and that the intrinsic magnitudes of the populations in the Galaxy and LMC may be different (van den Bergh 1995; Gould 1994).. The two distance scales appear to be in agreement, however, when Cepheids are compared with globular cluster horizontal branch magnitudes in M31 (Ajhar *et al.* 1996).

A positive value of  $s(R_0)$  such as we find indicates that the Sun’s orbit is elliptical with major axis in the quadrant  $0 < \phi < \pi/2$ , illustrated in Figure 10 (see also Schechter 1996). PMB suggest that the orbital ellipticity could be due to a bar of roughly 5 kpc radius, based on results of a numerical simulation; this is somewhat larger than the  $\lesssim 3$  kpc scale suggested by photometric observations (e.g. Weinberg 1992). The kinematic signature of the smaller-scale bar at  $R_0$  is predicted to be  $\lesssim 1\%$  in the models of Weinberg (1994), thus would be a strict lower limit for the scale of the bar if the outward motion of the LSR is such a kinematic signature. The B3 models in Table 8 with  $p < 0$  correspond to these inner bar models with ellipticity falling at  $R_0$ .

Our measurement of  $s(R_0)$  indicates that the Sun has a small outward velocity component with respect to the GC, of  $\Theta_R(R_0, 0) = 10.2 \pm 3.8 \text{ km s}^{-1}$  for our fiducial model B1. This model has  $p = 0$ , i.e. the ellipticity is constant with radius, which predicts that stars toward  $\ell = 180^\circ$  should have zero mean velocity. Observations of old disk stars at the anticenter, however, indicate a mean motion of  $\sim 6 \text{ km s}^{-1}$  in the sense that the LSR and the outer Galaxy stars are moving *apart* (Lewis & Freeman 1989, Metzger & Schechter 1994). This would suggest that  $s(R)$  increases with radius, such as might be the effect of a triaxial halo that gradually dominates an axisymmetric disk potential as  $R$  increases. Orbits at larger radius would thus have larger ellipticity, implying a larger  $\langle v_r \rangle$  (so long as  $\alpha \geq 0$ ), and would thus appear to have a net outward motion when viewed from inner orbits. This corresponds to models B3 with  $p > 0$ ; when we fit to these models, however, the magnitude of local ellipticity shrinks and becomes negligible with  $p = 1$ . The outward motion is consistent with the  $14 \text{ km s}^{-1}$  value of the Blitz & Spergel (1991a) model derived from outer Galaxy gas motions; however, warps and possible lopsided structure of the outer gas make the velocity structure difficult to interpret (Kuijken 1992).

One of the obstacles to drawing strong conclusions from models with different  $p$  and  $\alpha$  is that the distribution of the Cepheids in the model is both asymmetric with respect to the GC and concentrated about  $R = R_0$ . Constraining  $s(R)$  is best accomplished when the antisymmetric component can be measured directly on *both* sides of the Galactic center. To help fill out the region  $0 < \ell < 90^\circ$ , a survey for distant Cepheids has been conducted toward  $\ell = 60^\circ$  with some success (Metzger 1994). Further surveys are in progress to find Cepheids at even greater distances on the opposite side of the galaxy; if a sample of such Cepheids were available with radial velocities, good

constraints could also be placed on  $c(R)$  (KT).

It is clear that given the uncertainties in estimating total  $V$ -band extinction toward heavily obscured Cepheids (§3), the future direction of Cepheid kinematic models will be toward using infrared photometry. This will be particularly important for new samples of distant stars; as an example, some of the newly-discovered Cepheids toward  $\ell = 60^\circ$  have  $E(B-V)$  of  $\sim 4$  mag. An uncertainty in  $R_V$  of only 0.1 corresponds to a minimum distance error of 20%, while in  $K$  the corresponding extinction and error is reduced by a factor of 10. Future surveys for distant Cepheids, particularly those to find Cepheids at distances  $> R_0$ , are also best conducted in the infrared. The small scale height of Cepheids is of order that of the gas and dust in the disk, so the total extinction to such stars on the opposite side of the Galaxy is prohibitive in the optical.

## 6. Summary

We have obtained new  $\gamma$ -velocities for the eight Cepheids discovered by CKS, and combine these with  $K$ -band photometry of Schechter *et al.* 1992 for use in disk kinematic models. Using a catalog of Cepheid magnitudes, color excesses, and radial velocities collected from many sources, we examine Galactic rotation parameters in the context of both axisymmetric and non-axisymmetric models. In our adopted model, which assumes a flat rotation curve and constant ellipticity near the sun, we find

$$\begin{aligned} R_0 &= 7.66 \pm 0.32 \pm 0.44 \text{ kpc} , \\ v_c(R_0) &= 237 \pm 12 \pm 13 \text{ km s}^{-1} , \\ s(R_0) &= 0.043 \pm 0.016 , \\ A &= 15.5 \pm 0.4 \pm 1.2 \text{ km s}^{-1} \text{ kpc}^{-1} . \end{aligned}$$

The errors quoted are internal and systematic, respectively. An additional systematic error is also present from the unknown component of ellipticity that is symmetric about the sun-center line, but comparisons with recent measurements of  $R_0$  from RR Lyraes indicate that this component should be small. An estimate of  $R_0$  can also be made directly from 7 Cepheids near the solar orbit with infrared photometry, independent of the rotation speed, giving  $7.95 \pm 0.31$  kpc for zero ellipticity and  $7.61 \pm 0.30$  kpc for 4% ellipticity. There is good agreement between the new values and some previously published estimates, with significantly smaller uncertainty in the present results. Future progress in determining rotation curve scale and shape will rely on infrared searches and photometry, both to find more distant stars through heavy extinction and to measure the distances more accurately.

We thank the Director of the Carnegie Observatories, L. Searle, for use of the facilities at Las Campanas, and the assistance of F. Peralta and O. Duhalde at the telescope. This work was supported by NSF grants AST-8996139, AST-9015920, and AST-9215736.

## REFERENCES

- Ajhar, E. A., Grillmair, C. J., Lauer, T. R., Baum, W. A., Faber, S. M., Holtzman, J. A., Lynds, C. R., & O’Neil, E. J. 1996, *AJ*, 111, 1110
- Alcock, C., Allsman, R. A., Axelrod, T. S., Bennett, D. P., Cook, K. H., Freeman, K. C., Griest, K., Marshall, S. L., Peterson, B. A., & Pratt, M. R. 1995, *AJ*, 109, 1653
- Alves, D. R. *et al.* 1995, *BAAS*, 187, 102.03
- Avruch, I. M. 1991, M.S. Thesis, Massachusetts Institute of Technology.
- Backer, D. C., & Sramek, R. A. 1987, in *The Galactic Center*, AIP Conf. Proc 155, ed. D. Backer (New York: AIP), p. 163
- Bevington, P. R. 1969, *Data Reduction and Error Analysis for the Physical Sciences* (New York: McGraw-Hill)
- Binney, J., Gerhard, O. E., Stark, A. A., Bally, J., & Uchida, K. I. 1991, *MNRAS*, 252, 210
- Blitz, L., & Spergel, D. N. 1991a, *ApJ*, 370, 205
- Blitz, L., & Spergel, D. N. 1991b, *ApJ*, 379, 631
- Caldwell, J. A. R., & Coulson, I. M. 1987, *AJ*, 93, 1090 (CC)
- Caldwell, J. A. R., Keane, M. J., & Schechter, P. L. 1991, *AJ*, 101, 1763 (CKS)
- Caldwell, J., Avruch, I., Metzger, M., Schechter, P., & Keane, M. 1992, in *Variable Stars and Galaxies*, ed. B. Warner, ASP Conf. Ser. 30, 111.
- Carney, B. W., Storm, J., & Jones, R. V. 1992, *ApJ*, 386, 663 (CSJ)
- Carney, B. W., Fulbright, J. P., Terndrup, D. M., Suntzeff, N. B., & Walker, A. R. 1995, *AJ*, 110, 1674
- Clayton, J. A., Cardelli, G. C., & Mathis, J. S. 1989, *ApJ*, 345, 245
- Cohen, J. G., Frogel, J. A., Persson, S. E., & Elias, J. H. 1981, *ApJ*, 249, 481
- Coulson, I. M., & Caldwell, J. A. R. 1985, *MNRAS*, 216, 671
- Dean, J. F., Warren, P. R., & Cousins, A. W. J. 1978, *MNRAS*, 183, 569
- Delhaye, J. 1965, in *Galactic Structure*, eds. A. Blaauw & M. Schmidt (Chicago: U. of Chicago), p. 61
- Dwek, E., Arendt, R. G., Hauser, M. G., Kelsall, T., Lisse, C. M., Moseley, S. H., Silverberg, R. F., Soderoski, T. J., & Weiland, J. L. 1995, *ApJ*, 445, 716

- Elias, J. H., *et al.*. 1982, *AJ*, 87, 1029
- Evans, N. R. 1991, *ApJ*, 372, 597
- Feast, M. W. 1967, *MNRAS*, 136, 141
- Feast, M. W., & Walker, A. R. 1987, *ARA&A*, 25, 345
- Fernie, J. D. 1987, *AJ*, 94, 1003
- Fernie, J. D. 1990, *ApJS*, 72, 153
- Fernie, J. D. 1994, *ApJ*, 429, 824
- Fernie, J. D., Beattie, B., Evans, N. R., & Seager, S. 1995, *IBVS No.* 4148
- Fernie, J. D., & McGonegal, R. 1983, *ApJ*, 275, 732
- Gieren, W. P., Barnes, T. G., & Moffett, T. J. 1989, *ApJ*, 342, 467
- Gieren, W. P., & Fouqué, P. 1993, *AJ*, 106, 734
- Gould, A. 1994, *ApJ*, 426, 542
- Harris, H. C. 1985b, *AJ*, 90, 756
- Iben, I., & Renzini, A. 1984, *Phys. Rept.*, 105, 329
- Joy, A. H. 1939, *ApJ*, 89, 356
- Kraft, R. P., & Schmidt, M. 1963, *ApJ*, 137, 249
- Kuijken, K. 1992, *PASP*, 104, 809
- Kuijken, K., & Tremaine, S. 1994, *ApJ*, 421, 178 (KT)
- Laney, C. D., & Stobie, R. S. 1993a, *MNRAS*, 260, 408
- Laney, C. D., & Stobie, R. S. 1993b, *MNRAS*, 263, 921
- Laney, C. D., & Stobie, R. S. 1994, *MNRAS*, 266, 441
- LeDell, A. M. 1993, B.S. Thesis, Massachusetts Institute of Technology.
- Lewis, J. R., & Freeman, K. C. 1989, *AJ*, 97, 139
- McGonegal, R., McAlary, C. W., McLaren, R. A., & Madore, B. F. 1983, *ApJ*, 269, 641
- Madore, B. F., & Freedman, W. L. 1991, *PASP*, 103, 933

- Mateo, M., & Schechter, P. L. 1989, in 1<sup>st</sup> ESO/ST-ECF Data Analysis Workshop, eds. P. J. Grosbøl, F. Murtagh, & R. H. Warmels, p. 69
- Maurice, E., Mayor, M., Andersen, J., Ardeberg, A., Benz, W., Lindgren, H., Imbert, M., Martin, N., Nordström, B., & Prévot, L. 1984, *A&AS*, 57, 275
- Mayor, M. 1985, in *Stellar Radial Velocities*, eds. A. G. D. Phillip & D. W. Latham, p. 299
- Mermilliod, J. C., Mayor, M., & Burki, G. 1987, *A&A*, 70, 389
- Metzger, M. R., Caldwell, J. A. R., McCarthy, J. K., & Schechter, P. L. 1991, *ApJS*, 76, 803
- Metzger, M. R., Caldwell, J. A. R., & Schechter, P. L. 1992, *AJ*, 103, 529 (MCS)
- Metzger, M. R., & Schechter, P. L. 1994, *ApJ*, 420, 177
- Metzger, M. R. 1994, Ph.D. Thesis, Massachusetts Institute of Technology.
- Mihalas, D., & Binney, J. 1981, *Galactic Astronomy* (New York: Freeman)
- Moffett, T. J., & Barnes, T. G. 1985, *ApJS*, 58, 843
- Moffett, T. J., & Barnes, T. G. 1986, *MNRAS*, 219, 45P
- Moffett, T. J., & Barnes, T. G. 1987, *PASP*, 99, 1206
- Olson, B. I. 1975, *PASP*, 87, 349
- Pont, F., Mayor, M. & Burki, G. 1994, *A&A*, 285, 415 (PMB)
- Reid, M. J., Schneps, M. H., Moran, J. M., Gwinn, C. R., Genzel, R., Downes, D., & Roennaeng, B. 1988, *ApJ*, 330, 809
- Reid, M. J. 1993, *ARA&A*, 31, 345
- Rieke, G. H., & Lebofsky, M. J. 1985, *ApJ*, 288, 618
- Sargent, W. L. W., Schechter, P. L., Boksenberg, A., & Shortridge, K. 1977, *ApJ*, 212, 326
- Savage, B. D., & Mathis, J. D. 1979, *ARA&A*, 17, 73
- Schechter, P. L., Avruch, I. M., Caldwell, J. A. R., & Keane, M. J. 1992, *AJ*, 104, 1930
- Stibbs, D. W. N. 1956, *MNRAS*, 116, 453
- Stothers, R. B. 1988, *ApJ*, 329, 712
- Turner, D. G. 1976, *AJ*, 81, 1125

Turner, D. G. 1985, in *Cepheids: Theory and Observations*, ed. B. F. Madore (Cambridge: Cambridge), p. 209.

van den Bergh, S. 1995, *ApJ*, 446, 39

Walker, A. R., & Terndrup, D. M. 1991, *ApJ*, 378, 119

Walker, A. R. 1992, *ApJ*, 390, L81

Weinberg, M. 1992, *ApJ*, 384, 81

Weinberg, M. 1994, *ApJ*, 420, 597

Welch, D. L., Wieland, F., McAlary, C. W., McGonegal, R., Madore, B. F., McLaren, R. A., & Neugebauer, G. 1984, *ApJS*, 54, 547

Table 1. Radial Velocity Standards, Feb 91

Star	$V_r$	$\varepsilon_f$	$\varepsilon_V$	$n$
HD 24331	26.6	1.7	1.3	3
HD 39194	16.4	1.7	0.8	4
HD 48381	40.1	1.5	0.5	4
HD 83443	27.4	1.2	0.7	6
HD 83516	43.3	1.2	1.5	7
HD 101266	21.5	1.3	1.5	6
HD 111417	-18.9	1.2	0.8	7
HD 176047	-41.5	1.3	0.6	5
CPD -43° 2527	19.3	1.3	1.2	5
HD 74000	205.5	4.6	1.6	4
HD 140283	-171.2	3.2	3.6	3

Table 2. Cepheid Radial Velocities, Feb 91

JD	$V_r$	$\sigma$	JD	$V_r$	$\sigma$
-2400000	km s <sup>-1</sup>		-2400000	km s <sup>-1</sup>	
11447-6153			12003-6213		
48312.748	23.8	4.0	48312.730	-3.9	4.1
48313.649	31.0	3.6	48313.754	-12.3	3.8
48314.661	42.8	3.2	48314.770	-3.5	3.4
48315.651	52.0	4.3	48315.728	11.8	4.1
48316.726	11.3	5.3	48316.806	24.5	3.4
48317.612	13.9	5.2	48317.709	20.0	4.6
11465-6209			13190-6235		
48312.679	-12.4	5.7	48312.794	-35.4	3.8
48313.581	-13.9	4.6	48313.812	-22.6	4.0
48314.598	-2.7	3.0	48314.820	-14.2	3.1
48315.606	-15.4	4.4	48315.817	-8.5	4.3
48316.676	-18.5	4.0	48316.877	-24.5	4.3
48317.577	-0.4	3.5	48317.770	-45.4	4.7
11492-6257			13240-6245		
48312.847	10.2	7.3	48313.765	-7.5	3.7
48313.682	-6.1	4.3	48314.831	-9.4	3.8
48314.742	4.8	5.6	48315.880	-26.6	5.0
48315.712	20.0	6.6	48316.830	-32.2	5.7
48316.757	-6.7	5.2			
48317.676	-3.1	4.6			
11521-6200			13323-6224		
48312.693	31.4	4.4	48313.782	-39.7	4.8
48313.596	4.4	3.9	48314.851	-54.9	4.9
48314.695	12.6	3.6	48315.869	-53.3	4.5
48315.620	14.1	4.9	48316.847	-41.9	3.7
48316.701	19.9	3.1	48317.799	-37.2	4.5
48317.638	26.0	3.9			



Table 3. Gamma Velocities of New Cepheids

Cepheid	$\gamma$	$\sigma_{fit}$	$\sigma_{MC}$	$\chi^2_\nu$	Period <sup>a</sup>
11447-6153	29.1	2.0	1.9	1.5	6.4282
11465-6209	0.9:	4.0	3.8	4.4	11.0984
11492-6257	6.7	1.6	2.5	0.5	3.6798
11521-6200	20.4	1.7	1.7	1.2	6.6039
12003-6213	2.3	1.8	2.2	1.1	9.1266
13190-6235	-31.7	2.2	3.2	1.9	10.1576
13240-6245	-29.9:	3.3	8.6	0.6	15.0598
13323-6224	-48.3	3.0	2.1	2.2	4.2424

<sup>a</sup> Avruch (1991).

Table 4. Calculated Parameters for New Cepheids

Cepheid	Amp( $V$ )	$\langle K \rangle$	$\sigma_{\langle K \rangle}$	$JD_{Vmax}^a$	$JD_{Kmax}^a$	Period
11447-6153	0.65	10.092	0.013	7962.97	8337.43	6.4282
11465-6209	0.88	8.558	0.014	7968.7	8337.84	11.0984
11492-6257	0.62	10.649	0.009	7959.80	8336.00	3.6529
11521-6200	0.63	9.645	0.014	7958.40	8335.16	6.5763
12003-6213	0.72	9.125	0.012	7958.67	8339.86	9.0131
13190-6235	0.82	8.739	0.015	7958.76	8342.12	10.3001
13240-6245	1.21	7.618	0.022	7966.94	8337.60	15.2158
13323-6224	0.46	7.910	0.012	7961.75	8336.63	4.2424

<sup>a</sup> Modulo 2,440,000;  $\sigma \simeq 0.025 \times$  period.

Table 5. Cepheid Data

Cepheid	$\ell$	$b$	$v_r^a$	$\log P$	$\langle V \rangle^{b,c}$	E(B-V)	
AQL	ETA	40.90	-13.10	-14.8	0.8559	3.897	0.164
AQL	U	30.90	-11.60	1.1	0.8466	6.448	0.389
AQL	SZ	35.60	-2.30	10.5	1.2340	8.617	0.607
AQL	TT	36.00	-3.10	1.9	1.1384	7.147	0.476
AQL	FF	49.20	6.40	-17.4	0.6504	5.372	0.232
AQL	FM	44.30	0.90	-7.0	0.7863	8.268	0.611
AQL	FN	38.50	-3.10	13.1	0.9769	8.382	0.489
AQL	V336	34.20	-2.10	11.5	0.8636	9.875	0.610
AQL	V496	28.20	-7.10	7.9	0.8330	7.720	0.402
AQL	V600	43.90	-2.60	3.1	0.8597	10.034	0.812
ARA	V340	335.20	-3.70	-82.2	1.3183	10.242	0.547
AUR	Y	166.80	4.30	8.5	0.5865	9.614	0.385
AUR	RT	183.10	8.90	21.0	0.5715	5.450	0.076
AUR	RX	165.80	-1.30	-23.3	1.0654	7.664	0.278
AUR	SY	164.70	2.10	-3.5	1.0062	9.081	0.439
CMA	RW	232.00	-3.80	50.0	0.7581	11.146	0.520
CMA	RY	226.00	0.30	32.9	0.6701	8.105	0.253
CMA	RZ	231.20	-1.10	24.6	0.6289	9.698	0.448
CMA	SS	239.20	-4.20	73.1	1.0921	9.939	0.524
CMA	TV	227.20	-2.40	39.0	0.6693	10.566	0.555
CMA	TW	229.20	0.10	66.5	0.8448	9.557	0.351
CMA	VZ	239.90	-4.40	40.1	0.4950	9.371	0.466
CAM	RW	144.90	3.80	-26.5	1.2152	8.657	0.614
CAM	RX	145.90	4.70	-36.2	0.8983	7.685	0.542
CAR	1	283.20	-7.00	3.6	1.5507	3.735	0.183
CAR	U	289.10	0.10	1.7	1.5883	6.281	0.285
CAR	V	275.30	-12.30	13.9	0.8258	7.375	0.187
CAR	Y	285.70	-0.30	-14.5	0.5611	8.102	0.190
CAR	SX	286.70	1.30	-11.4	0.6866	9.100	0.323
CAR	UW	285.60	-1.80	-14.4	0.7280	9.441	0.441
CAR	UX	284.80	0.20	8.1	0.5661	8.266	0.141
CAR	UY	287.20	-3.20	4.0	0.7438	8.928	0.200
CAR	UZ	287.30	-2.30	-20.9	0.7164	9.331	0.198
CAR	WW	288.20	0.00	-13.0	0.6700	9.794	0.388
CAR	WZ	289.20	-1.20	-14.7	1.3619	9.255	0.376
CAR	XX	291.30	-4.90	-10.9	1.1963	9.341	0.344
CAR	XY	291.40	-3.90	-5.6	1.0946	9.334	0.405
CAR	XZ	290.30	-0.80	1.5	1.2214	8.595	0.360
CAR	YZ	285.60	-1.40	1.0	1.2592	8.709	0.386

Table 5—*Continued*

Cepheid	$\ell$	$b$	$v_r^a$	$\log P$	$\langle V \rangle^{b,c}$	E(B-V)
CAR AQ	285.80	-3.30	2.1	0.9899	8.821	0.175
CAR CC	289.40	-1.60	6.9	0.6776	12.021	0.503
CAR CF	289.40	-1.60	-3.8	0.7400	12.400	0.602
CAR CN	283.60	-1.30	9.0	0.6931	10.670	0.407
CAR CQ	286.20	-1.70	20.6	0.7258	13.400	0.902
CAR CR	285.70	-0.40	25.3	0.9895	11.566	0.484
CAR CS	288.60	0.20	10.8	0.8236	12.400	0.702
CAR CY	289.50	-0.90	8.6	0.6300	9.782	0.380
CAR DY	288.80	-1.00	-1.3	0.6698	11.394	0.382
CAR ER	290.10	1.50	-19.0	0.8876	6.807	0.121
CAR FF	286.90	0.60	-14.5	1.2130	12.300	0.900
CAR FH	288.40	-1.30	14.0	0.7531	12.500	0.700
CAR FI	287.80	0.70	13.2	1.1289	11.655	0.683
CAR FK	288.70	-0.40	29.9	1.3665	12.200	0.900
CAR FM	289.90	-1.00	39.7	0.8830	12.400	0.800
CAR FN	289.60	-0.10	-13.0	0.6614	11.623	0.553
CAR FO	290.50	-2.10	-10.8	1.0152	10.773	0.445
CAR FQ	290.90	-0.40	-3.1	1.0117	11.821	0.811
CAR FR	291.10	0.60	-7.3	1.0301	9.675	0.346
CAR FZ	288.40	0.30	-1.6	0.5536	11.600	0.619
CAR GI	290.30	2.50	-20.6	0.6465	8.320	0.188
CAR GS	289.20	-1.80	32.1	0.6080	12.500	0.700
CAR GZ	284.70	-1.90	-8.5	0.6190	10.239	0.407
CAR HS	285.30	-1.80	5.9	0.7069	12.300	0.700
CAR IM	289.10	-0.80	3.8	0.7272	12.300	0.700
CAR IO	289.30	-0.90	39.3	1.1337	10.938	0.453
CAR IT	291.50	-1.10	-14.9	0.8770	8.094	0.204
CAS RS	114.50	0.80	-24.5	0.7991	9.928	0.818
CAS RW	129.00	-4.60	-71.3	1.1702	9.224	0.408
CAS RY	115.30	-3.30	-70.5	1.0840	9.957	0.614
CAS SU	133.50	8.50	-7.0	0.2898	5.970	0.288
CAS SW	109.70	-1.60	-38.0	0.7357	9.700	0.475
CAS SY	118.20	-4.10	-47.1	0.6097	9.858	0.448
CAS SZ	134.80	-1.20	-45.9	1.1344	9.852	0.767
CAS UZ	125.50	-1.60	-51.0	0.6293	11.351	0.498
CAS VV	130.40	-2.10	-50.5	0.7930	10.751	0.528
CAS VW	124.60	-1.10	-58.5	0.7777	10.708	0.458
CAS XY	122.80	-2.80	-42.0	0.6534	9.979	0.534
CAS AP	120.90	0.10	-44.5	0.8355	11.528	0.781

Table 5—*Continued*

Cepheid	$\ell$	$b$	$v_r^a$	$\log P$	$\langle V \rangle^{b,c}$	E(B-V)
CAS BP	125.40	2.80	-46.5	0.7974	10.916	0.883
CAS CD	115.50	1.10	-54.9	0.8922	10.746	0.766
CAS CF	116.60	-1.10	-77.7	0.6880	11.126	0.539
CAS CG	116.80	-1.30	-79.3	0.6401	11.355	0.663
CAS DD	116.80	0.50	-70.1	0.9918	9.878	0.481
CAS DF	136.00	1.50	-33.0	0.5834	10.856	0.569
CAS DL	120.30	-2.60	-38.1	0.9031	8.964	0.510
CAS FM	117.80	-6.20	-29.1	0.7641	9.128	0.346
CAS V636	127.50	1.10	-24.9	0.9231	7.186	0.786
CEN V	316.40	3.30	-23.2	0.7399	6.820	0.290
CEN TX	315.20	-0.60	-52.0	1.2328	10.537	0.982
CEN UZ	295.00	-0.90	-11.9	0.5230	8.760	0.278
CEN VW	307.60	-1.60	-30.8	1.1771	10.242	0.433
CEN XX	309.50	4.60	-18.8	1.0397	7.799	0.264
CEN AY	292.60	0.40	-15.5	0.7251	8.820	0.309
CEN AZ	292.80	-0.20	-11.5	0.5066	8.635	0.174
CEN BB	296.40	-0.70	-15.8	0.6017	10.146	0.386
CEN BK	298.00	-1.00	-26.3	0.5016	10.063	0.327
CEN IZ	294.90	-0.50	-19.7	0.7703	12.500	0.800
CEN KK	294.20	2.70	-2.7	1.0856	11.502	0.608
CEN KN	307.80	-2.10	-39.7	1.5317	9.855	0.654
CEN LV	294.30	-1.70	-16.7	0.6968	12.100	0.700
CEN MY	305.30	1.20	-15.2	0.5704	12.018	1.158
CEN MZ	305.40	-1.60	-30.6	1.0151	11.546	0.852
CEN OO	306.90	-0.60	-35.7	1.1099	12.004	1.107
CEN QY	311.90	-0.20	-58.7	1.2492	11.796	1.398
CEN V339	313.50	-0.50	-24.4	0.9762	8.689	0.415
CEN V378	306.10	0.30	-16.5	0.8102	8.464	0.386
CEN V381	310.80	4.40	-31.8	0.7058	7.659	0.214
CEN V419	292.10	4.30	-15.2	0.7410	8.181	0.188
CEP DELTA	105.20	0.50	-17.4	0.7297	3.954	0.113
CEP AK	105.10	0.40	-45.6	0.8593	11.186	0.664
CEP CP	100.40	1.10	-40.5	1.2518	10.619	0.644
CEP CR	107.60	0.30	-32.3	0.7947	9.629	0.712
CIR AX	315.80	4.00	-25.5	0.7221	5.880	0.167
CRU R	299.60	1.10	-16.5	0.7654	6.771	0.203
CRU S	303.30	4.40	-7.1	0.6712	6.599	0.177
CRU T	299.40	0.40	-9.8	0.8282	6.570	0.204
CRU X	302.30	3.80	-25.0	0.7938	8.357	0.287

Table 5—*Continued*

Cepheid	$\ell$	$b$	$v_r^a$	$\log P$	$\langle V \rangle^{b,c}$	E(B-V)
CRU SU	299.20	-0.60	-33.6	1.1088	9.822	0.930
CRU SV	296.80	-0.40	-15.4	0.8453	12.130	0.790
CRU TY	298.00	-0.20	-14.3	0.6980	11.700	0.800
CRU VV	299.90	-1.80	-35.1	0.7868	12.300	1.301
CRU VW	300.90	-0.70	-2.7	0.7214	9.602	0.638
CRU VX	300.90	1.60	-28.5	1.0868	12.007	0.891
CRU AD	298.50	0.50	-34.3	0.8060	11.037	0.642
CRU AG	301.70	3.10	-8.5	0.5840	8.204	0.220
CRU BG	300.40	3.40	-20.3	0.5241	5.462	0.078
CYG X	76.90	-4.30	8.3	1.2145	6.396	0.289
CYG SU	64.80	2.50	-21.4	0.5850	6.857	0.116
CYG SZ	84.40	4.00	-12.1	1.1792	9.434	0.598
CYG TX	84.40	-2.30	-20.4	1.1676	9.515	1.093
CYG VX	82.20	-3.50	-18.0	1.3038	10.073	0.742
CYG VY	82.90	-4.60	-11.9	0.8953	9.590	0.617
CYG VZ	91.50	-8.50	-18.5	0.6871	8.957	0.290
CYG BZ	84.80	1.40	-13.2	1.0061	10.232	0.870
CYG CD	71.10	1.40	-11.6	1.2323	8.957	0.493
CYG DT	76.50	-10.80	-1.6	0.3978	5.774	0.065
CYG GH	66.50	-0.10	-11.1	0.8931	9.937	0.626
CYG MW	70.90	-0.60	-16.4	0.7749	9.485	0.642
CYG V386	85.50	-4.90	-5.1	0.7207	9.631	0.836
CYG V402	74.10	2.30	-12.7	0.6400	9.871	0.405
CYG V438	77.60	2.30	-10.2	1.0496	10.939	1.200
CYG V459	90.50	0.70	-20.7	0.8604	10.601	0.748
CYG V520	87.50	1.60	-22.8	0.6073	10.853	0.752
CYG V532	89.00	-3.00	-16.2	0.5164	9.090	0.511
CYG V1334	83.60	-8.00	-5.2	0.5226	5.885	-0.037
CYG V1726	92.51	-1.61	-15.3	0.6269	9.011	0.311
DOR BETA	271.70	-32.80	7.3	0.9931	3.755	0.070
GEM ZETA	195.70	11.90	6.8	1.0066	3.918	0.046
GEM W	197.40	3.40	-0.1	0.8985	6.951	0.285
GEM RZ	187.70	-0.10	12.0	0.7427	10.016	0.543
GEM AA	184.60	2.70	9.5	1.0532	9.735	0.327
GEM AD	193.30	7.60	45.0	0.5784	9.858	0.180
GEM BB	199.40	2.30	64.3	0.3632	11.364	0.444
GEM DX	198.10	2.80	16.0	0.4964	10.742	0.436
LAC V	106.50	-2.60	-25.4	0.6976	8.939	0.350
LAC X	106.50	-2.50	-25.3	0.7359	8.407	0.356

Table 5—*Continued*

Cepheid	$\ell$	$b$	$v_r^a$	$\log P$	$\langle V \rangle^{b,c}$	E(B-V)
LAC Y	98.70	-4.00	-22.0	0.6359	9.150	0.225
LAC Z	105.80	-1.60	-30.0	1.0369	8.418	0.394
LAC RR	105.60	-2.00	-38.8	0.8073	8.844	0.348
LAC BG	93.00	-9.30	-18.6	0.7269	8.878	0.332
LUP GH	324.90	3.30	-16.1	0.9678	7.633	0.358
MON T	203.60	-2.60	22.0	1.4317	6.129	0.218
MON SV	203.70	-3.70	27.1	1.1828	8.260	0.254
MON TX	214.10	-0.80	51.0	0.9396	10.965	0.490
MON TY	213.40	1.20	59.5	0.6055	11.400	0.700
MON TZ	214.00	1.30	34.0	0.8709	10.775	0.427
MON XX	215.50	-1.10	66.4	0.7370	11.898	0.566
MON AA	217.10	-0.30	66.1	0.5953	13.300	0.779
MON BE	204.90	1.00	45.4	0.4322	10.579	0.590
MON CV	208.60	-1.80	18.9	0.7309	10.306	0.673
MON EE	220.00	3.80	68.9	0.6821	12.500	0.469
MON FG	221.70	-0.10	88.7	0.6529	12.900	1.000
MON FI	221.50	1.00	85.8	0.5169	12.931	0.515
MON V465	214.90	3.70	60.7	0.4334	10.380	0.260
MON V508	208.90	0.90	58.8	0.6164	10.551	0.321
MUS R	302.10	-6.50	0.1	0.8756	6.285	0.138
MUS S	299.60	-7.50	-1.7	0.9849	6.123	0.162
MUS RT	296.50	-5.30	-5.5	0.4894	8.977	0.325
MUS TZ	296.60	-3.00	-24.6	0.6942	11.759	0.657
MUS UU	296.80	-3.20	-17.0	1.0658	9.772	0.402
NOR S	327.80	-5.40	5.8	0.9892	6.430	0.200
NOR U	325.60	-0.20	-21.8	1.1018	9.249	0.833
NOR RS	329.10	-1.20	-40.5	0.7923	10.035	0.552
NOR SY	327.50	-0.70	-32.9	1.1019	9.472	0.745
NOR TW	330.40	0.30	-56.6	1.0328	11.670	1.234
NOR GU	330.50	-1.70	-24.5	0.5382	10.425	0.646
NOR QZ	329.44	-02.12	-38.6	0.7300	8.866	0.278
NOR V340	329.72	-02.27	-40.0	1.0526	8.381	0.332
OPH Y	20.60	10.10	-6.6	1.2336	6.167	0.620
OPH BF	9.90	7.10	-29.0	0.6094	7.331	0.252
ORI RS	196.60	0.30	40.5	0.8789	8.412	0.380
ORI CR	195.90	-3.90	22.4	0.6912	12.296	0.538
ORI CS	198.00	-4.50	15.5	0.5898	11.390	0.392
ORI GQ	199.80	-4.30	43.9	0.9353	8.965	0.281
PER SV	162.60	-1.50	-4.5	1.0465	8.989	0.421

Table 5—*Continued*

Cepheid	$\ell$	$b$	$v_r^a$	$\log P$	$\langle V \rangle^{b,c}$	E(B-V)
PER SX	158.90	-6.40	5.5	0.6325	11.166	0.471
PER UX	133.60	-3.10	-41.5	0.6595	11.608	0.514
PER UY	135.90	-1.40	-45.0	0.7296	11.339	0.857
PER VX	132.80	-3.00	-35.4	1.0372	9.305	0.494
PER VY	135.10	-1.70	-39.5	0.7429	11.255	0.877
PER AS	154.14	-0.88	-25.5	0.6966	9.726	0.672
PER AW	166.60	-5.40	6.9	0.8104	7.486	0.511
PER V440	135.90	-5.20	-26.1	0.8791	6.247	0.276
PUP X	236.10	-0.80	65.3	1.4143	8.490	0.429
PUP RS	252.40	-0.20	22.1	1.6169	7.028	0.431
PUP VW	235.36	-00.62	+24.0	0.6320	11.382	0.493
PUP VX	237.00	-1.30	8.8	0.4789	8.315	0.152
PUP VZ	243.40	-3.30	63.3	1.3648	9.595	0.454
PUP WX	241.20	-1.40	54.6	0.9512	9.058	0.317
PUP WZ	241.80	3.30	64.0	0.7013	10.301	0.228
PUP AQ	246.20	0.00	59.5	1.4774	8.755	0.491
PUP AT	254.30	-1.60	26.7	0.8238	8.001	0.195
PUP BM	244.50	-1.00	64.4	0.8573	10.811	0.581
PUP BN	247.90	1.00	65.7	1.1359	9.922	0.424
PUP HW	244.80	0.80	116.2	1.1288	12.129	0.681
PUP LS	246.40	0.10	77.4	1.1506	10.363	0.460
PUP MY	261.30	-12.90	12.7	0.7555	5.666	0.088
SGE S	55.20	-6.10	-10.1	0.9233	5.622	0.144
SGE GY	54.90	-0.60	15.6	1.7107	10.208	1.268
SGR U	13.70	-4.50	2.6	0.8290	6.714	0.393
SGR W	1.60	-4.00	-28.3	0.8805	4.669	0.130
SGR X	1.20	0.20	-13.7	0.8458	4.561	0.207
SGR Y	12.80	-2.10	-2.5	0.7614	5.742	0.214
SGR VY	10.13	-01.07	-6.0	1.1322	11.529	1.185
SGR WZ	12.10	-1.30	-15.7	1.3395	8.030	0.450
SGR XX	15.00	-1.90	2.0	0.8078	8.851	0.519
SGR YZ	17.80	-7.10	18.5	0.9742	7.350	0.293
SGR AP	8.10	-2.40	-15.0	0.7040	6.942	0.203
SGR AV	7.50	-0.60	0.0	1.1878	11.425	1.170
SGR AY	13.30	-2.40	-26.5	0.8176	10.520	0.857
SGR BB	14.70	-9.00	7.6	0.8220	6.931	0.286
SGR V350	13.80	-8.00	13.1	0.7114	7.460	0.311
SGR V773	2.90	-0.50	-0.9	0.7597	12.387	1.488
SGR V1954	10.56	-1.73	12.7	0.7909	10.861	0.818

Table 5—*Continued*

Cepheid	$\ell$	$b$	$v_r^a$	$\log P$	$\langle V \rangle^{b,c}$	E(B-V)
SCO RV	350.40	5.70	-16.6	0.7825	7.041	0.338
SCO RY	356.50	-3.40	-17.7	1.3077	8.016	0.729
SCO KQ	340.40	-0.70	-22.1	1.4575	9.810	0.836
SCO V470	349.80	0.30	-2.8	1.2112	10.934	1.633
SCO V482	354.40	0.20	10.7	0.6559	7.973	0.354
SCO V500	359.00	-1.40	-10.8	0.9693	8.753	0.569
SCO V636	343.50	-5.20	8.3	0.8323	6.651	0.225
SCT X	19.00	-1.60	0.0	0.6230	10.011	0.587
SCT Y	24.00	-0.90	12.3	1.0146	9.659	0.771
SCT Z	26.80	-0.80	37.2	1.1106	9.595	0.518
SCT RU	28.40	0.20	-4.8	1.2944	9.465	0.891
SCT SS	24.20	-1.80	-8.6	0.5648	8.201	0.333
SCT TY	28.05	+00.12	+25.5	1.0435	10.791	0.943
SCT UZ	19.16	-01.49	+38.8	1.1686	11.303	0.994
SCT BX	28.90	-1.70	-2.4	0.8069	12.231	1.216
SCT CK	26.30	-0.50	-0.4	0.8701	10.608	0.746
SCT CM	27.20	-0.40	40.8	0.5930	11.101	0.724
SCT CN	28.10	0.00	19.7	0.9997	12.470	1.170
SCT EV	23.50	-0.50	17.5	0.4901	10.136	0.641
SCT V367	21.60	-0.80	-8.4	0.7989	11.604	1.186
SER AA	30.80	1.80	-44.3	1.2340	12.234	1.318
TAU ST	193.10	-8.10	0.5	0.6057	8.199	0.350
TAU SZ	179.50	-18.70	0.3	0.4982	6.530	0.295
TRA R	317.00	-7.80	-13.2	0.5301	6.650	0.144
TRA S	322.10	8.20	3.9	0.8009	6.394	0.120
TRA U	323.20	-8.00	-13.1	0.4098	7.940	0.109
UMI ALPHA	123.30	26.50	-17.4	0.5988	1.973	0.024
VEL T	265.50	-3.80	5.7	0.6665	8.030	0.283
VEL V	276.60	-4.20	-27.9	0.6406	7.570	0.218
VEL RZ	262.90	-1.90	24.1	1.3096	7.087	0.332
VEL ST	268.80	-4.80	7.4	0.7677	9.707	0.483
VEL SV	286.00	2.40	3.5	1.1491	8.576	0.383
VEL SW	266.20	-3.00	22.9	1.3706	8.126	0.344
VEL SX	265.50	-2.20	30.9	0.9800	8.290	0.255
VEL XX	284.80	2.20	15.0	0.8442	10.662	0.545
VEL AB	283.00	0.60	28.1	0.7956	13.500	1.301
VEL AE	276.10	-0.60	14.8	0.8533	10.254	0.630
VEL AH	262.40	-7.00	24.2	0.4953	5.708	0.097
VEL AP	263.00	-1.40	26.3	0.4953	10.053	0.494



Table 5—*Continued*

Cepheid	$\ell$	$b$	$v_r^a$	$\log P$	$\langle V \rangle^{b,c}$	E(B-V)
VEL AX	263.30	-7.70	22.1	0.4140	8.200	0.232
VEL BG	271.90	-2.60	7.9	0.8404	7.662	0.433
VEL BH	259.80	-1.30	51.6	0.8574	11.600	1.300
VEL CP	267.60	-3.20	73.9	0.9930	12.756	0.855
VEL CS	277.09	-0.77	26.8	0.7712	11.688	0.792
VEL CX	272.40	-3.40	16.0	0.7962	11.370	0.713
VEL DD	271.50	-1.40	26.0	1.1204	12.536	0.911
VEL DP	275.40	-1.30	29.8	0.7391	11.825	0.892
VEL DR	273.20	1.30	20.6	1.0492	9.526	0.647
VEL EX	274.10	-2.20	33.5	1.1217	11.567	0.763
VEL EZ	274.93	-01.94	+92.2	1.5383	12.440	1.091
VUL T	72.10	-10.20	-0.9	0.6469	5.749	0.088
VUL U	56.10	-0.30	-12.1	0.9026	7.127	0.619
VUL X	63.80	-1.30	-16.1	0.8007	8.848	0.793
VUL SV	63.90	0.30	1.9	1.6542	7.208	0.543
VUL DG	64.90	-0.90	2.6	1.1338	11.375	1.167

<sup>a</sup> See text for references

<sup>b</sup> Caldwell & Coulson (1987) and references therein

<sup>c</sup> Pont *et al.* (1994)

Table 6. Axisymmetric Model Parameters

Model		$2AR_0$ km s <sup>-1</sup>	$m_0$ mag	$u_0$ km s <sup>-1</sup>	$v_0$ km s <sup>-1</sup>	$\delta v_r$ km s <sup>-1</sup>	$R_0$ kpc
A1	$n = 294$	241	10.45	-9.5	14.1	3.2	8.13
All Data		±13	±0.11	±1.3	±1.1	±0.9	±0.42
A1.1	$n = 288$	247	10.42	-8.8	13.9	2.9	8.02
Pruned		±12	±0.09	±1.2	±1.0	±0.8	±0.35
A1.2	$n = 288$	253	10.35	-8.4	13.7	2.9	7.76
F90 $E_{B-V}$		±12	±0.09	±1.2	±1.0	±0.8	±0.35
A2	$n = 184$	225	10.40	-8.6	12.8	3.2	7.94
CC Data		±19	±0.19	±1.5	±1.3	±1.0	±0.72
A2.1	$n = 184$	236	10.40	-7.0	13.2	3.1	
New $v_r$		±19	±0.17	±1.4	±1.2	±0.9	
A2.2	$n = 184$	227	10.30	-8.2	12.6	3.3	
F90 $E_{B-V}$		±19	±0.17	±1.4	±1.2	±0.9	
A2.3	$n = 184$	240	10.32	-6.5	12.7	3.3	7.66
Both New		±19	±0.17	±1.4	±1.2	±0.9	±0.60
A3	$n = 266$	255	10.42	-9.7	13.6	0.0	8.02
PMB Data		±13	±0.12	±1.2	±1.1		±0.46
A3.1	$n = 266$	247	10.33	-9.4	13.9	2.2	7.69
PMB w/ $\delta v_r$		±13	±0.11	±1.2	±1.0	±0.8	±0.40

Table 7. Axisymmetric Model Covariances

		$2AR_0$ km s <sup>-1</sup>	$m_0$ mag	$u_0$ km s <sup>-1</sup>	$v_0$ km s <sup>-1</sup>	$\delta v_r$ km s <sup>-1</sup>	$R_0$ kpc
Model A1.1	$n = 288$	247	10.42	-8.8	13.9	2.9	8.02
Pruned		$\pm 12$	$\pm 0.09$	$\pm 1.2$	$\pm 1.0$	$\pm 0.8$	$\pm 0.35$
	$2AR_0$	1.00	0.80	0.22	0.25	-0.20	
	$m_0$		1.00	0.18	0.38	-0.23	
	$u_0$			1.00	-0.03	0.13	
	$v_0$				1.00	0.13	
Model A1.4	$n = 280$	253	10.47	-8.7	14.1	2.8	8.20
No New		$\pm 14$	$\pm 0.12$	$\pm 1.2$	$\pm 1.0$	$\pm 0.8$	$\pm 0.47$
	$2AR_0$	1.00	0.86	0.22	0.29	-0.20	
	$m_0$		1.00	0.18	0.39	-0.22	
	$u_0$			1.00	-0.01	0.12	
	$v_0$				1.00	0.11	
Model A2	$n = 184$	225	10.40	-8.6	12.8	3.2	7.94
CC Data		$\pm 19$	$\pm 0.19$	$\pm 1.5$	$\pm 1.3$	$\pm 1.0$	$\pm 0.72$
	$2AR_0$	1.00	0.88	0.22	0.27	-0.09	
	$m_0$		1.00	0.17	0.31	-0.14	
	$u_0$			1.00	0.06	0.24	
	$v_0$				1.00	0.18	

Table 8. Non-Axisymmetric Models

Model		$v_c$ km s <sup>-1</sup>	$m_0$ mag	$u_0$ km s <sup>-1</sup>	$v_0$ km s <sup>-1</sup>	$s(R_0)$	$R_0$ kpc
B1	$n = 288$	237	10.32	-9.3	13.5	0.043	7.66
Pruned		±12	±0.09	±1.1	±1.0	±0.016	±0.32
B1.1	$n = 288$	242	10.26	-8.8	13.3	0.044	7.45
F90 $E_{B-V}$		±12	±0.09	±1.1	±1.0	±0.016	±0.32
B2.1	$R_{v,0} = 2.97$	235	10.37	-9.3	13.5	0.044	7.83
B2.2	$R_{v,0} = 3.17$	239	10.30	-9.1	13.5	0.043	7.59
B3.1	$p = -1.0$	235	10.32	-8.7	13.6	0.046	
B3.2	$p = -0.5$	235	10.31	-9.0	13.6	0.047	
B3.3	$p = +0.5$	246	10.40	-9.3	13.2	0.021	
B3.4	$p = +1.0$	257	10.51	-9.1	13.0	0.004	
B3.5	$\alpha = -0.2$	197	10.32	-9.4	14.1	0.071	
B3.6	$\alpha = -0.1$	216	10.33	-9.3	13.8	0.055	
B3.7	$\alpha = +0.1$	262	10.32	-9.1	13.2	0.034	
B3.8	$\alpha = +0.2$	293	10.30	-9.0	12.9	0.027	

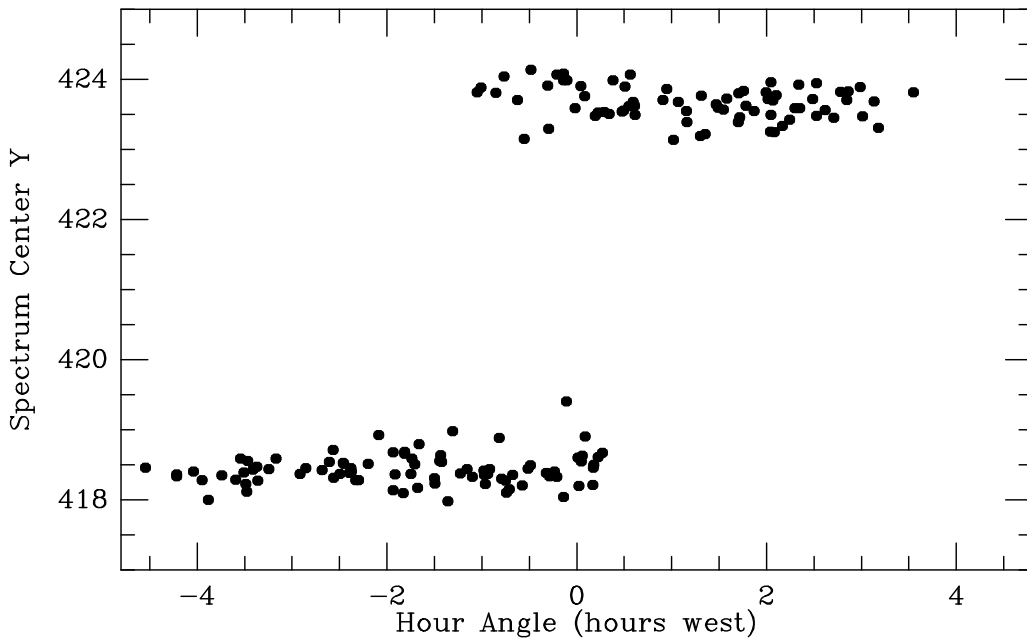


Fig. 1.— The pixel location of the center of the spectrum, along the cross-dispersed direction, plotted as a function of telescope hour angle. A significant shift is seen near the meridian (with some hysteresis), possibly caused by motion of the grism.

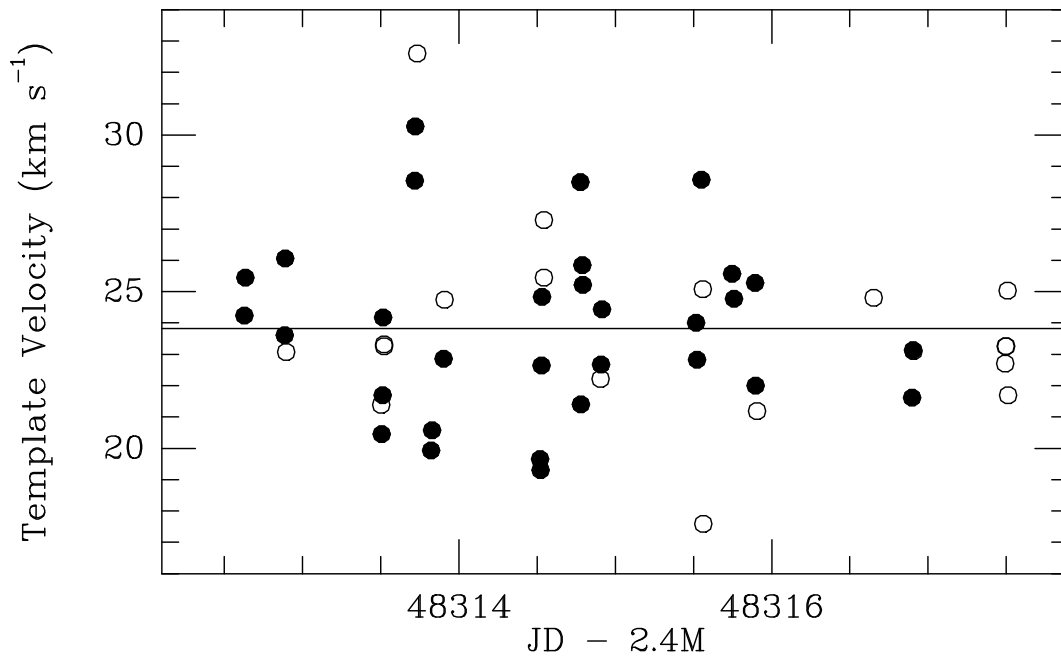


Fig. 2.— Velocities of the template calculated from spectra of radial velocity standards. The open and filled points correspond to velocities measured from the two different locations of the spectrum on the chip; the error of each measurement is typically  $2.7 \text{ km s}^{-1}$ . The solid line shows the adopted mean velocity for the template.

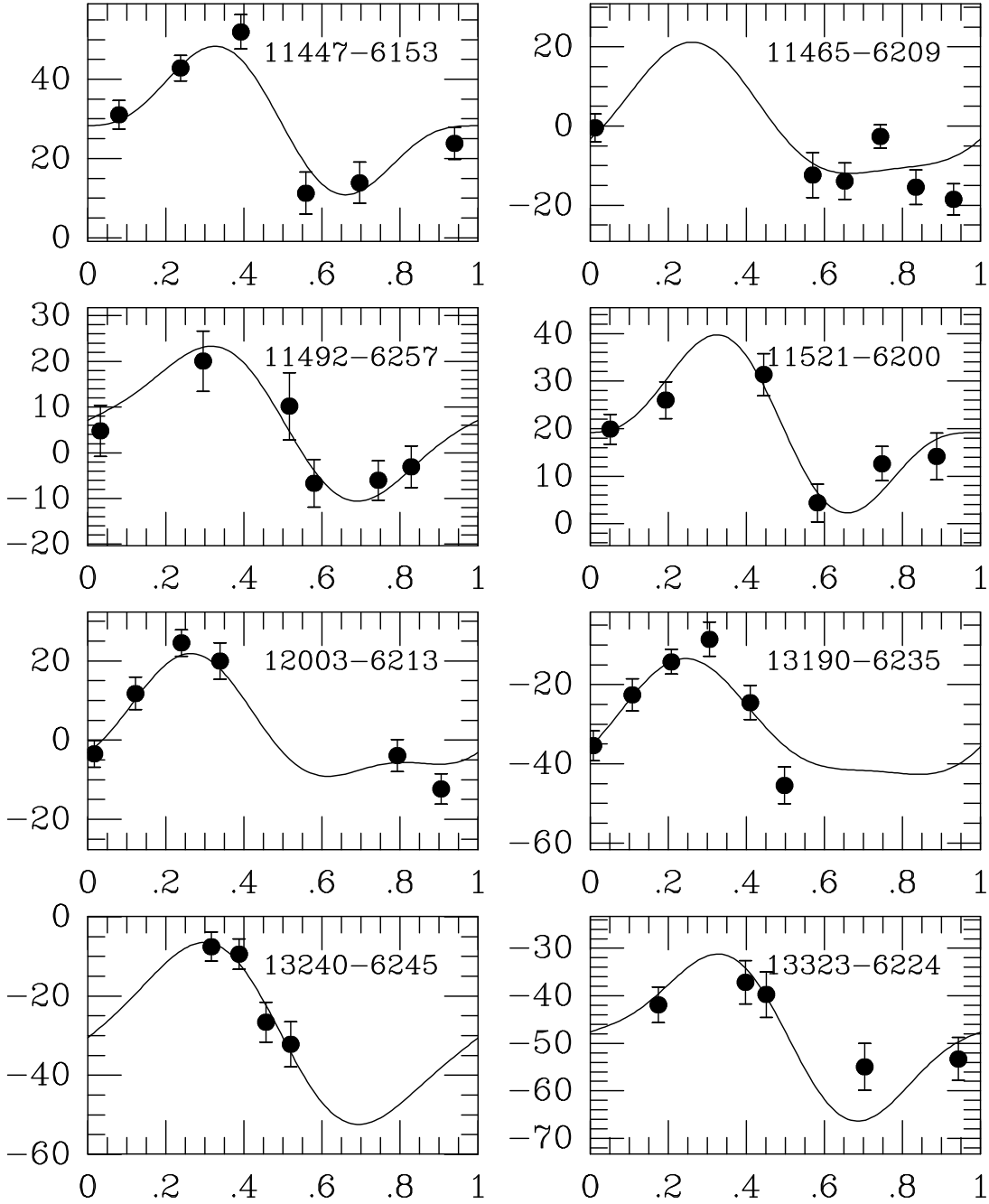


Fig. 3.— Radial velocity curves for the newly discovered Cepheids, using the designations of Caldwell *et al.*. The curve shape was determined from the period, and its position in phase and  $\gamma$  velocity were fit to the radial velocities shown.

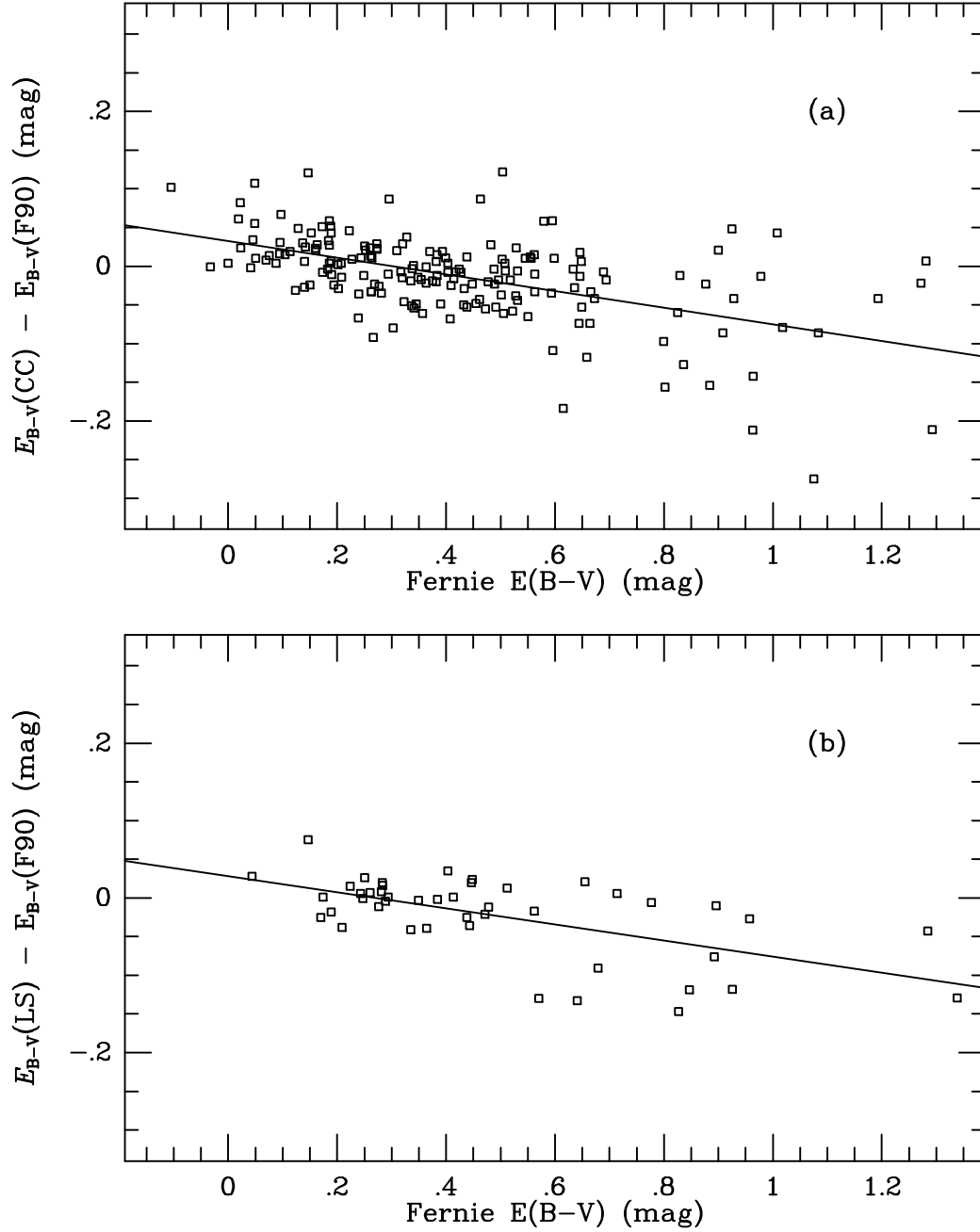


Fig. 4.— A comparison of the reddenings from Fernie (1990) and (a) Caldwell & Coulson (1987); (b) Laney & Stobie 1994. A linear fit to each is shown, revealing a reddening scale difference in both.



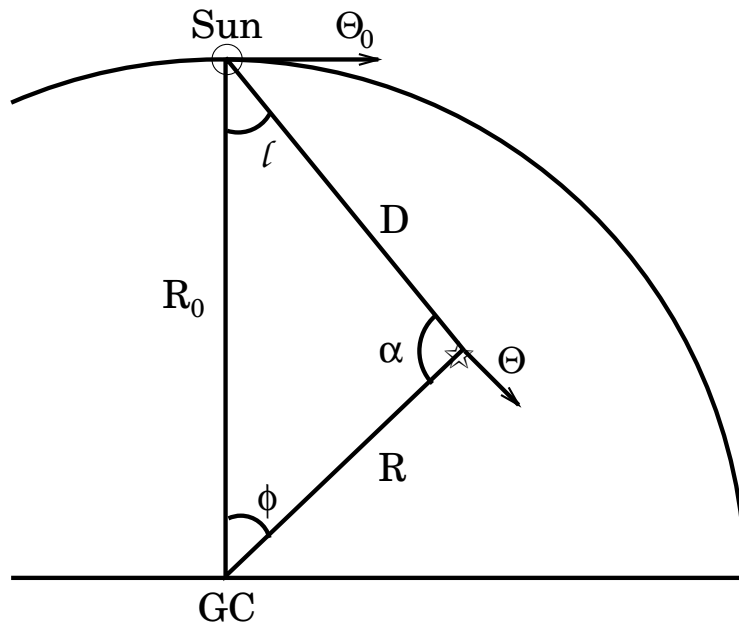


Fig. 5.— A schematic of Milky Way rotation, with labels indicating quantities discussed in the text. The sun is indicated with a circle near the top of the figure, and a fiducial Cepheid is indicated with a star. The Galactic center is labeled GC.

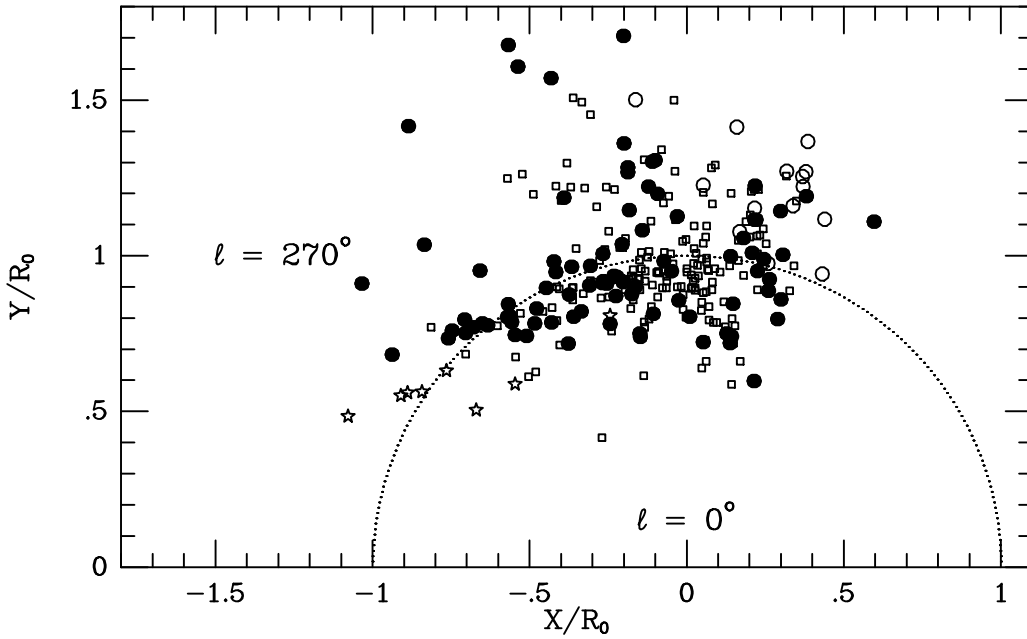


Fig. 6.— Locations of Milky Way Cepheids used in the rotation curve models. Squares indicate Cepheids modeled by CC. Open circles indicate additional Cepheids with new reddenings, filled circles Cepheids with new radial velocities from MCS and PMB, and stars indicate Cepheids newly discovered by Caldwell *et al.*. Cartesian coordinates are shown in units of  $R_0$  with the Galactic center at  $(0,0)$  and the Sun at  $(0,1)$ . The solar circle ( $r = 1$ ) is shown with a dotted line.

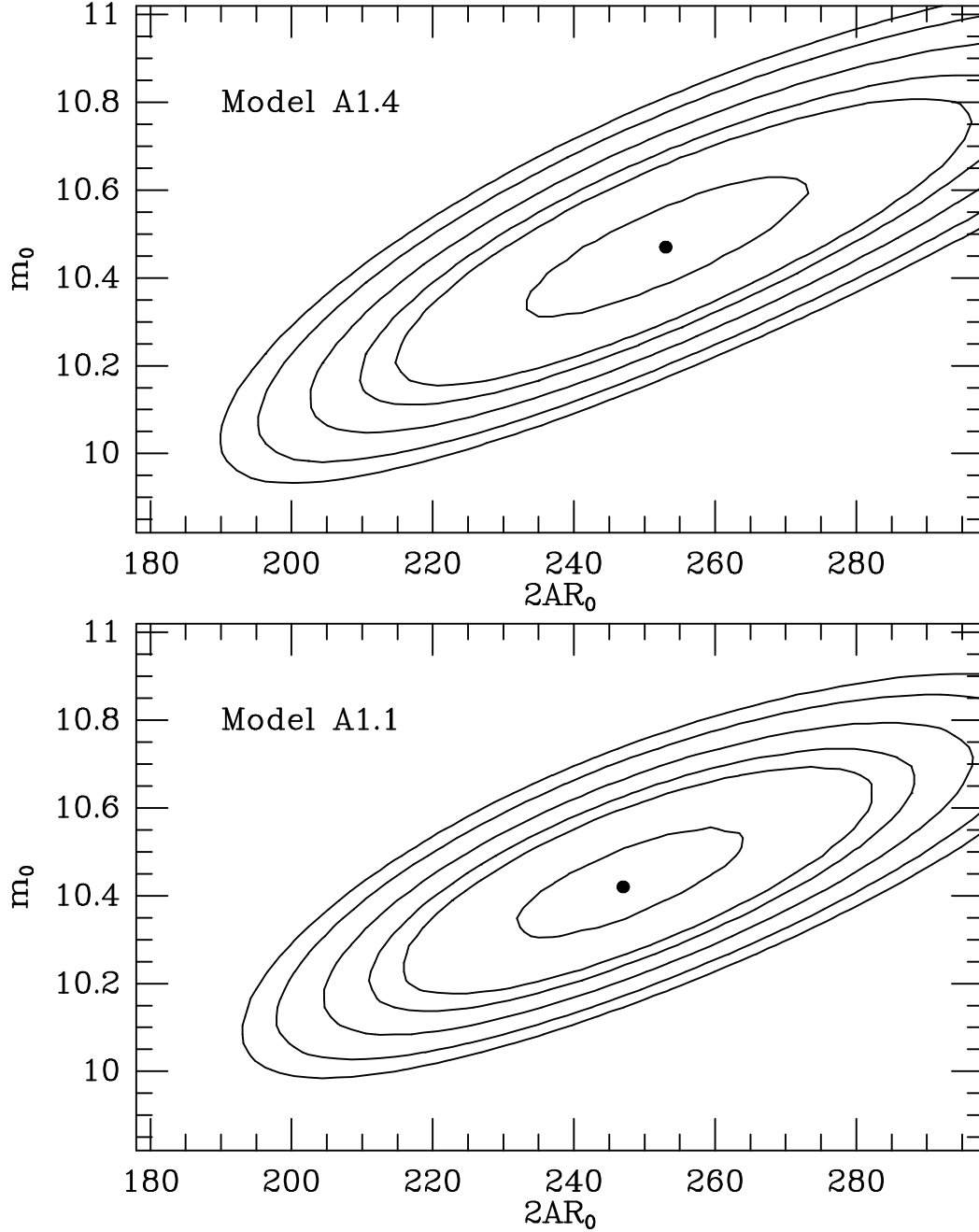


Fig. 7.— Constant  $\delta\chi^2$  contours for two models projected in the  $2AR_0, m_0$  plane. Contours shown are (from inside to outside) 1- $\sigma$ , 90%, 2- $\sigma$ , 99%, 99.9%, and 99.99%. The top panel is a model using all Cepheids with  $V$ -band data. The bottom panel is a model that also includes CKS Cepheids, where distances were determined from  $K$ -band data.

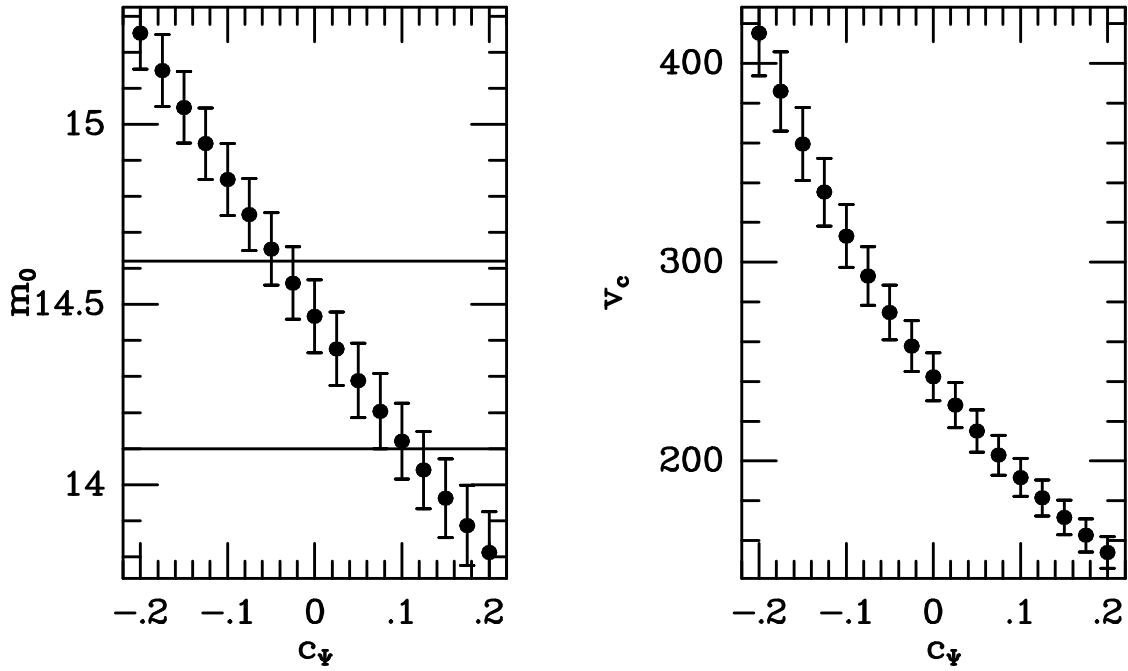


Fig. 8.— A plot of the best-fit model parameters as a function of the symmetric ellipticity component  $c(R_0)$ . The left panel shows the fit distance modulus of the galactic center,  $(m - M)_0$ , the right panel circular velocity. A flat rotation curve and constant ellipticity are assumed. The two horizontal lines represent  $1\text{-}\sigma$  errors on other, non-kinematic distance measurements (Reid 1993).

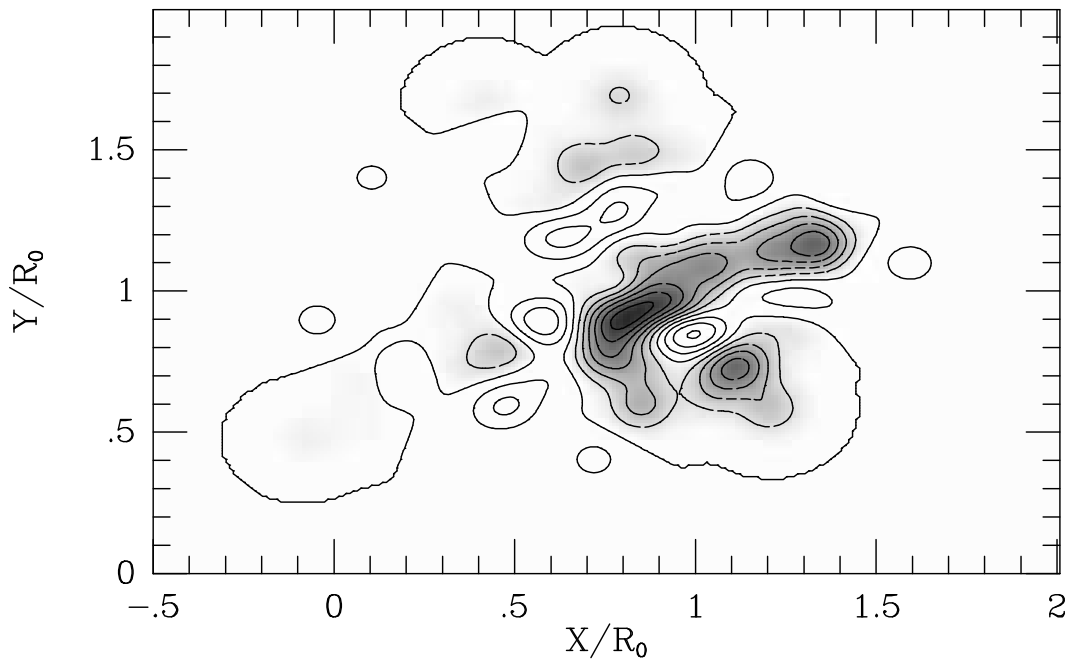


Fig. 9.— Residual velocities of the stars in Model B1, smoothed with a 0.5 kpc gaussian filter. Contour levels are at  $2 \text{ km s}^{-1}$  increments. Shaded contours are negative velocity residuals, i.e. the mean motion of stars in these areas is toward the sun with respect to the model.

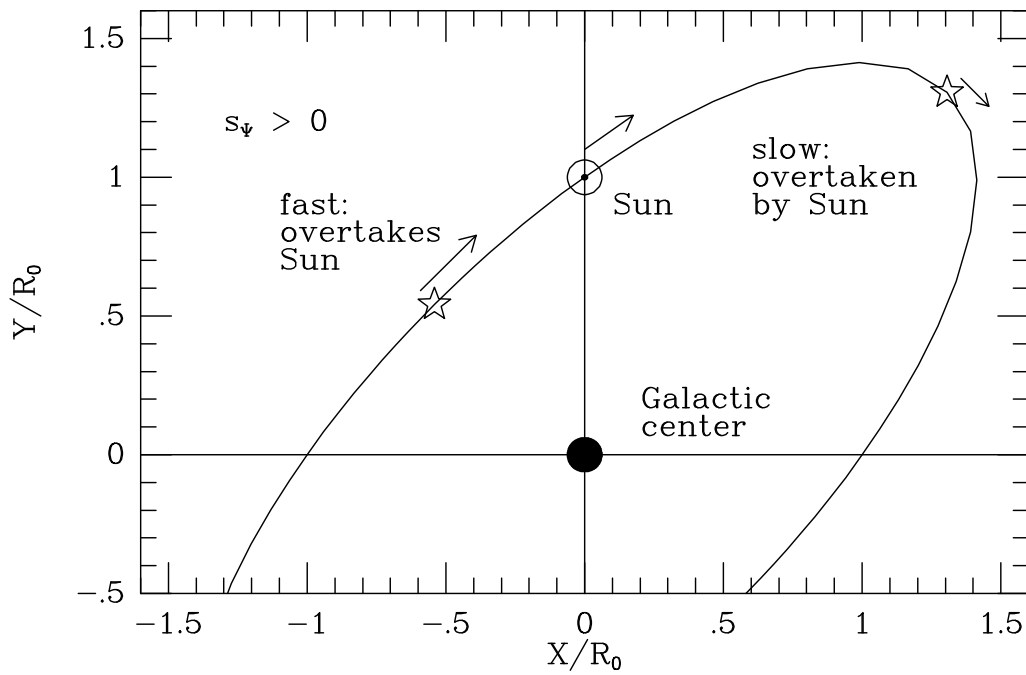


Fig. 10.— A schematic of the closed elliptical orbits that pass through the sun in our fiducial model. The general orientation of the orbits is depicted; the ellipticity has been exaggerated for clarity.